IDO-16958
March 1964

AEC
RESEARCH REPORTS

RESULTS OF ATR SAMPLE FUEL PLATEL IRRADIATION EXPERIMENT

M. J. Graber, G. W. Gibson,
V. A. Walker, and W. C. Francis

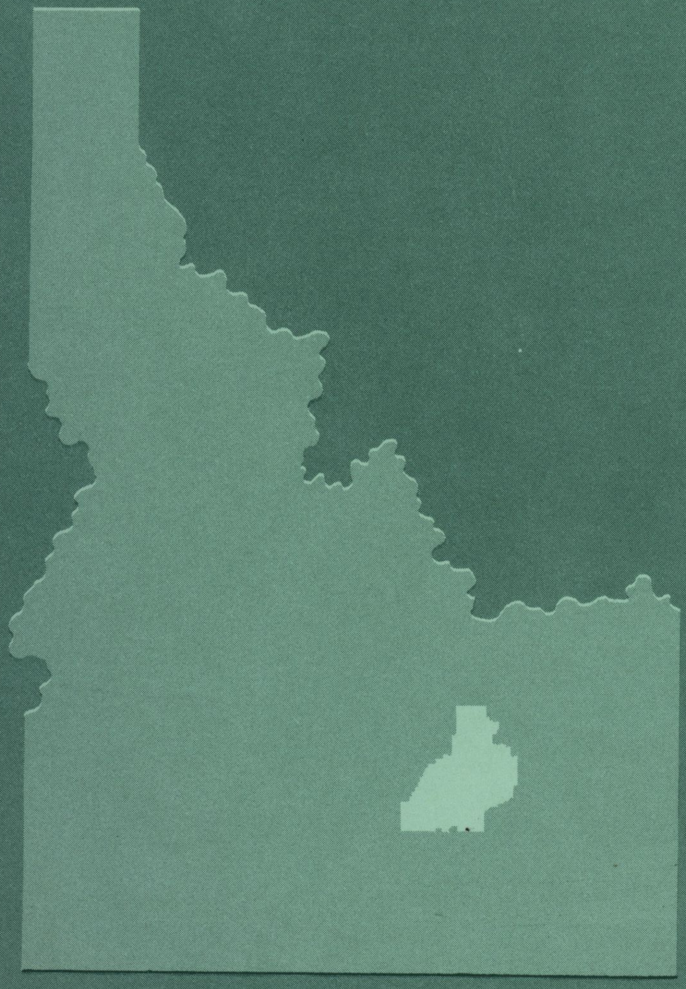

PHILLIPS PETROLEUM COMPANY

ATOMIC ENERGY DIVISION

NATIONAL REACTOR TESTING STATION
US ATOMIC ENERGY COMMISSION

PRICE $1.50

AVAILABLE FROM THE
OFFICE OF TECHNICAL SERVICES
U. S. DEPARTMENT OF COMMERCE
WASHINGTON 25, D. C.

PRINTED IN USA

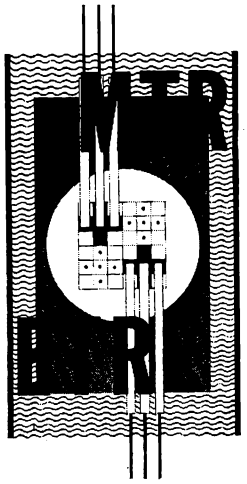

IDO-16958
AEC Research and Development Report
Metals, Ceramics and Materials
TID-4500 (26th Ed.)
Issued: March 23, 1964

RESULTS OF ATR SAMPLE FUEL PLATE IRRADIATION EXPERIMENT

BY

M. J. Graber
G. W. Gibson
V. A. Walker
W. C. Francis

PHILLIPS
PETROLEUM
COMPANY

Atomic Energy Division
Contract AT(10-1)-205
Idaho Operations Office
U. S. ATOMIC ENERGY COMMISSION

ACKNOWLEDGMENT

The authors and staff appreciate the many suggestions from the ORNL and B and W Atomic Energy Divisions. Also the work of the ICPP Analytical Laboratory and the Hot Cell Branches is to be acknowledged, particularly in those areas where other than routine analyses, tests, sample handling, and metallography were achieved.

ABSTRACT

Fuel materials proposed for use in the Advanced Test Reactor were evaluated. Aluminum alloy (X8001) cermet cores with UO_2, U_3O_8, or UAl_3 dispersants clad with either 6061-O or X8001 were irradiated in the Engineering Test Reactor at simulated Advanced Test Reactor conditions. Fabrication methods, test parameters, pre-irradiation and post-irradiation examinations are discussed. A core failure mechanism which produced blistering in the uranium oxide compositions was not detectable in the intermetallic compositions.

RESULTS OF ATR SAMPLE FUEL PLATE IRRADIATION EXPERIMENT

SUMMARY

This report summarizes the results of an irradiation experiment to examine the behavior of fuels and cladding materials being considered for use in the Advanced Test Reactor. Fuel materials consisted of 35 and 44 weight percent U_3O_8, 32 and 41 weight percent UO_2, and 40 and 54 weight percent UAl_3. In all cases the core matrix material was X-8001 aluminum alloy containing 0.19 weight percent B_4C. The cladding material was X-8001 aluminum alloy with 10 percent cold work on some samples and 6061-0 on the remainder. Electrolyzed samples of 6061-T6 aluminum alloy and 304 stainless steel were included in the test piece. Design parameters for the experiment were (a) fuel plate surface temperature (maximum) at beginning of irradiation of 170°C, (b) thermal neutron flux of 2.5×10^{14} n/cm^2-sec, and (c) total burnup of 7×10^{20} fiss/cc. Sample fuel plates 2-5/16 x 2-7/8 x 0.050 inches were anodized for thermal barrier purposes, and irradiated in a core piece in the Engineering Test Reactor for two cycles beginning April 13, 1963, and terminating June 24, 1963. The electrolyzed materials study was extended for an additional three cycles of irradiation using fresh coupons.

All of the fuel samples were dimensionally stable for one cycle of irradiation (a maximum of $6\text{-}7 \times 10^{20}$ fiss/cc on some samples) although metallographic examination showed reaction between the uranium oxide fuel particles and the aluminum matrix. At the end of two cycles of irradiation (11.0×10^{20} fiss/cc maximum on some samples) all of the high fuel density U_3O_8 and UO_2 specimens had blistered, although, no fission product release was detected in the reactor process water. UAl_3 samples containing the same amount of U-235 and irradiated under the same conditions to the same burnup showed no evidence of failure. Metallographic examination of the oxide fuel samples showed large void formation and core separation. In the corresponding samples of UAl_3 the voids were small, well dispersed, and showed no evidence of interconnecting. The assessment of a realistic final surface temperature was complicated by uncertainties in the anodized coating thickness and thermal conductivity; but, the best estimate for maximum surface temperature appears to be 155 to 210°C.

The irradiation stability of the electrolyzed stainless steel samples was satisfactory to 8×10^{20} n/cm^2 (> 1 MeV) while the electrolyzed coating on the aluminum samples corroded at 4×10^{20} n/cm^2.

A second series of irradiations under more controlled conditions is currently planned for a water loop in the ETR. Design objectives for this test are (a) maximum heat flux of 2.25×10^6 Btu/hr-ft^2, (b) maximum thermal flux of 3.8×10^{14} n/cm^2-sec, (c) starting surface temperature of 170°C (without anodization), and (d) burnup of 7 and 12 x 10^{20} fiss/cc. To accomplish this test a new loop facility is being designed with construction scheduled to be completed the latter part of FY 1964.

RESULTS OF ATR SAMPLE FUEL PLATE
IRRADIATION EXPERIMENT

CONTENTS

FIGURES

TABLES

RESULTS OF ATR SAMPLE FUEL PLATE IRRADIATION EXPERIMENT

I. INTRODUCTION

In the conceptual design [1] for the Advanced Test Reactor it was recognized that the operating conditions would impose severe requirements on fuel and construction materials beyond that of MTR-ETR technology. In order to support the ATR design, a research and development program would be necessary to select adequate, if not optimum, materials. No operating experience was available at the levels of heat flux, fission rate, and temperature imposed on the fuel materials. Because of the high fuel density (eg, 30 weight percent U-235) and the burnable poison requirement, there was considerable doubt if the uranium-aluminum alloy fuels could be fabricated with satisfactory homogeneity and acceptable reject rate. Oxide fuels had been fabricated to even higher fuel loadings than required for the ATR and irradiated to suitable burnups (eg, 7×10^{20} fiss/cc) [2] at lower temperatures, heat flux, and fission rates. Phillips, therefore, strongly urged that at least a limited test be made with reference materials at conditions approaching as nearly as possible those of the ATR. In March 1962, at a meeting of interested parties* in Idaho Falls, proposals for irradiation testing of ATR fuel element samples were discussed. It was generally expected at that time that this would be merely a proof test of the reference fuel (with some alternate materials included) under conditions approximating those of the ATR. Because no suitable loop facility was available for the test, it was decided to irradiate sample plates in an ETR core piece along the lines established in the MTR for Phillips PAED-24 experiment [2].

In December 1962, Phillips Petroleum Co. outlined an irradiation program to test not only the U_3O_8-Al reference fuel for the ATR but also UO_2-Al and UAl_3-Al compositions as backup materials. Because the total fuel loading for the ATR was not yet firm and because there was a possibility that thermal analysis might dictate a zone-loaded fuel element, it was decided to test each of the above materials at 125 percent of the nominal U-235 content (based on 35 weight percent U_3O_8 in December 1962, but later increased to 41 weight percent U_3O_8). Again, because design studies at the time of planning for the irradiation experiment had not yet firmly established the operating temperature of the fuel plate, both X-8001 with 10 percent cold work and 6061 in the annealed condition were to be tested as cladding material.

A last minute addition to the experimental program was the inclusion of electrolyzed specimens of stainless steel and aluminum. The electrolyzing of these materials had been specified in those reactor components subjected to appreciable wear from moving contact. Out-of-pile corrosion and wear resistance for electrolyzed materials were reported to be excellent but their performance under irradiation was uncertain.

The samples with their ETR and ETRC holders were ready for reactor test as the PAED-59 experiment by April 1963, and all, except some extended irradiations on electrolyzed coupons, completed by the end of June 1963. Hot cell examinations and chemical analyses were essentially completed by the end of September 1963. The following sections of this report present details of the irradiation program and summarize the results of the work.

---

*B and W, ORNL, AEC-DRD, AEC-IDO, and Phillips Petroleum Co.

II. SAMPLE PREPARATION

1. SAMPLE FUEL PLATES

The sample fuel plate compositions used for the experiment are listed in Table 1. Figure 1 shows the details of the sample plate construction. In Tables II and III the details of the materials used for the fabrication of the sample fuel plates are given. The aluminum alloy materials used in the fuel plates were supplied to Phillips Petroleum Co. by ORNL. These were taken from the stocks of materials which were obtained for the development of fabrication procedures for the ATR fuel element. In making the sample plates every effort was made to duplicate the fabrication procedures developed at ORNL for fabrication of full size ATR plates.

The uranium-aluminum intermetallic compound was made by vacuum induction melting in a graphite crucible. Magnesium zirconate was used as a protective coating on the crucible. The molten alloy was cast into a mold consisting of a small clay-graphite crucible which had also been coated with magnesium zirconate. The cast material was crushed and then ground by ball milling.

The boron carbide powder used in all of the plates was supplied by ORNL. This powder had a particle size of -325 mesh.

TABLE I

ATR SAMPLE IRRADIATION PROGRAM -- SAMPLE COMPOSITIONS

Comp. No.	Core/Composition	Core Thickness (in.)	Aluminum Cladding Material	Cladding Thickness (in.)
ATR 1	35 wt% U_3O_8, Fully Enriched U, +0.19 wt% B_4C + X-8001 Al	0.020	X-8001 - 10% cw	0.015
ATR 2	32 wt% UO_2, Fully Enriched U, +0.19 wt% B_4C + X-8001 Al	0.020	X-8001 - 10% cw	0.015
ATR 3	40 wt% UAl_3, Fully Enriched U, +0.19 wt% B_4C + X-8001 Al	0.020	X-8001 - 10% cw	0.015
ATR 4	54 wt% UAl_3, Fully Enriched U, +0.19 wt% B_4C + X-8001 Al	0.020	6061-0	0.015
ATR 5	44 wt% U_3O_8, Fully Enriched U, +0.19 wt% B_4C + X-8001 Al	0.020	6061-0	0.015
ATR 6	41 wt% UO_2, Fully Enriched U, +0.19 wt% B_4C + X-8001 Al	0.020	6061-0	0.015
ATR 7	35 wt% U_3O_8, Fully Enriched U, +0.19 wt% B_4C + X-8001 Al	0.020	6061-0	0.015
ATR 8	32 wt% UO_2, Fully Enriched U, +0.19 wt% B_4C + X-8001 Al	0.020	6061-0	0.015
ATR 9	40 wt% UAl_3, Fully Enriched U, +0.19 wt% B_4C + X-8001 Al	0.020	6061-0	0.015
ETR 10	22 wt% UAl Alloy, Fully Enriched U	0.020	1100-0	0.015
ETR 11	35 wt% UAl_3, Fully Enriched U + Al powder	0.020	1100-0	0.015

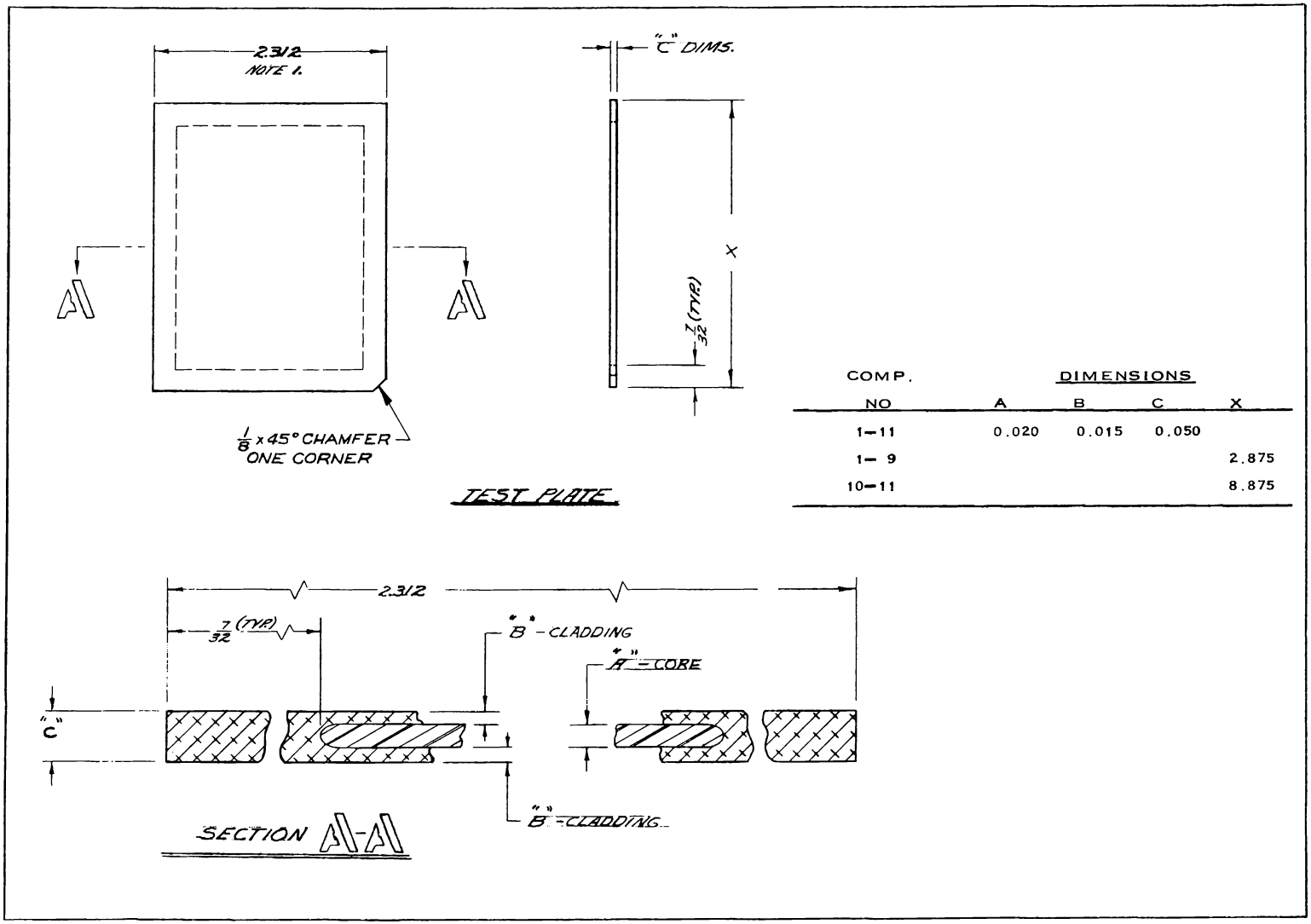

COMP. NO	DIMENSIONS A	B	C	X
1–11	0.020	0.015	0.050	
1– 9				2.875
10–11				8.875

Fig. 1 Fuel development program standard test plate details.

TABLE II

ATR FUEL IRRADIATION PROGRAM FUEL MATERIALS ANALYSIS

Fuel Material Source Grade	U_3O_8 Union Carbide Nuclear Co. Enriched U_3O_8	UO_2 United Nuclear Corp. High Fired, 93 wt% Enriched	UAl_3 Phillips Petroleum Co. Heat 264	U-Al Alloy Phillips Petroleum Co. Heat 262
U (wt%)	84.63	86.05	66.15	22.26
U-235 (%)	93.13	93.02	91.68	93.05
Al (ppm)	6	30	Balance	Balance
B	< 0.1	1	< 20	< 50
Ba	< 10	Nil	--	--
Be	0.01	Nil	--	--
C	12	Not Reported	1320	Not Reported
Ca	< 50	Nil	--	3
Cd	< 0.1	Nil	--	Not Reported
Co	< 1	Nil	--	Not Reported
Cr	10	50	< 3.5	50
Cu	13	200	< 26	265
Fe	40	1100	300	1700
Li	< 0.2	Not Reported	--	Not Reported
Mg	12	20	< 5	150
Mn	< 5	10	4	30
Mo	Not Reported	Nil	--	--
Ni	< 25	50	53	20
O	Balance	Balance	Not Reported	Not Reported
Pb	Not Reported	< 1	--	Not Reported
Si	< 10	70	66	620
Sn	< 10	< 4	--	300
Ti	--	7000	--	< 100
V (ppm)	< 1	Nil	--	Not Reported
X-Ray Diffractic Results	Not Reported	Not Reported	UAl_3 is the major crystalline compound. A very small amount of an unidentified substance is present. This could be UAl_4 and/or Al.	Not Reported
Mesh Size	-100 +325	-100 +325	-140	--

The atomized X-8001 aluminum alloy powder which had been vacuum annealed at one micron for four hours at 560°C was supplied by ORNL. This had a particle size of -100 mesh. The 6061 aluminum used for the cladding material was Alclad with 1100 aluminum on one side. The 6061 picture frame material was Alclad on both sides. The thickness of the Alclad layers was five percent of the total plate thickness.

The powders for the sample fuel plate cores, after being weighed, were blended dry in glass jars for three hours prior to compacting. The blended powders were compacted with a double acting press using a compacting pressure of 33 tsi to form core compacts measuring 1-7/8 x 1/2 x 1/10 inch. Stearic acid dissolved in methanol was used as the die lubricant for this operation.

After being vacuum annealed for two hours at a temperature of 590°C under a vacuum of 50 microns the cores were assembled into picture frames with the 1/2 inch dimension of the cores parallel to the rolling direction.

In compositions ETR 10 and 11 the vacuum annealing step for the cores was omitted. In the plates for these compositions the three core compacts were assembled side by side with the 1-7/8 inch dimension parallel to the rolling direction. The core alloy for composition ETR 10 was made by induction melting in air, casting into a copper mold, and hot rolling to the desired thickness.

TABLE III

ATR FUEL IRRADIATION PROGRAM ALUMINUM BASE FUEL PLATE MATERIALS ANALYSIS

Material Spectral Analysis (%)	1100 Al Cladding	6061 Al	X-8001 Sheet	X-8001 Powder
Si	0.082	0.54	0.091	0.01
Fe	0.47	0.38	0.42	0.39
Mn	0.016	0.014	0.007	0.01
Cu	0.086	0.26	0.007	0.006
Mg	0.00096	0.11	0.0014	0.001
Cr	Nil	0.18	Nil	Nil
Ni	≈ 0.005	≈ 0.005	0.90	1.20
Ti	0.012	0.025	0.007	0.001
Pb	≈0.01	≈ 0.01	0.01	0.01
Ga	≈ 0.05	≈ 0.05	≈ 0.05	≈ 0.05
Zn	Nil	Nil	Nil	Nil
B	< 0.005	< 0.005	< 0.005	< 0.005

In all of the compositions the cover plates were fastened to the picture frames by means of a single rivet located at the leading edge of the assembly.

The fuel plate assemblies were preheated for 3/4 hour at 500°C and then hot rolled using a mill with eight-inch diameter rolls. A reduction in thickness of 20 percent per pass was made during the hot rolling with a five minute reheat time between each pass. The hot rolling was stopped when the plates approached 110 percent the final thickness. At this time a one hour blister anneal at a temperature of 590°C was performed. After inspection for blistering the plates were given a 10 percent cold reduction to the final thickness. The 6061 clad plates were then given a final anneal for one hour at 500°C.

These procedures resulted in a 5:1 reduction ratio in fabrication of the plates. The plates were roll leveled following the cold rolling passes and radiographed to locate the cores. Finally, the plates were sheared to size.

2. THERMAL BARRIER COATING

In order to raise the fuel plate surface temperatures of the samples being tested in the ETR to the levels expected in the ATR it was necessary to apply a thermal barrier coating. The requirements for this coating were that it have a low thermal conductivity, a low thermal neutron absorption cross section, and an

adherence to the surface of sample fuel plates. Al_2O_3 applied by anodizing was chosen as the material meeting these requirements.

After fabrication and inspection, the samples plates to be irradiated were sent to the Sylcor Division of Sylvania Electric Products Inc., Hicksville, New York, for anodizing. The "Marcoat" hard coat anodizing process was used. In this process, a mixture of oxalic and sulfuric acids was used (at fairly low temperature, 10°C) for the electrolyte. A current density of 36 amps per ft^2 and a potential of 10 to 75 volts was used. After the electrolytic treatment, the films were sealed by placing the plates in boiling water.

According to the literature, [3], this process should produce a porous film. The outer layer of the film should be thin and be boehmite (α-AlO(OH). However, X-ray diffraction examination of the films failed to detect boehmite.

The coating thickness applied to the samples was measured by Sylcor using a Dermitron instrument. A set of blank aluminum plates anodized in the same manner by Sylcor was checked by Dermitron and metallographic measurements. These data are shown in Table IV.

TABLE IV

COMPARISON OF COATING THICKNESS MEASUREMENTS

Plate No.	Alloy	Sylcor Measurement	P.P.Co. Measurement	
		Dermitron (mils)	Dermitron (mils)	Metallograph (mils)
2	X-8001	0.5	0.9	--
3	X-8001	1.0	1.1	1.1
4	X-8001	1.5	1.6	--
5	X-8001	2.0	1.8	--
7	1100	0.5	1.0	1.0
8	1100	1.0	1.3	1.2
9	1100	1.5	1.7	--
10	1100	2.0	2.2	2.0
12	6061	0.5	0.8	--
13	6061	1.0	1.2	--
14	6061	1.5	1.6	1.6
15	6061	2.0	2.3	--

From these data it would appear that there is a good correlation between the Dermitron and metallographic measurements made by Phillips Petroleum Co., and that there is a good relation between the Phillips and Sylcor measurements

in the coatings one mil thick or over. However, the specified 0.5 mil coatings were almost twice as thick when measured at Phillips Petroleum Co.

The fuel plate samples of compositions ETR 10 and 11 were not anodized as these were to be irradiated under ambient ETR conditions. Also, plate number E-13, a composition ATR 1 plate which was inserted for the last half of the irradiation, was not anodized.

III. TEST ENVIRONMENT

1. EXPERIMENT DESIGN

1.1 Mechanical Design

To satisfy the experimental irradiation objectives, it was apparent that irradiation in the core of the Engineering Test Reactor was necessary since the desired combination of thermal neutron flux and fuel plate temperature could not be obtained in any other existing facility. Accordingly, the design was initiated on the basis of replacing a standard ETR fuel element with the sample fuel plate core piece. Figure 2 shows the design of this piece.

The external geometry of the core piece was a duplicate of an ETR fuel element to assure that the piece would have no adverse effects upon adjacent ETR fuel elements. Provision for regulating total flow through the piece was made by the installation of an orifice plate at the top of the bottom end box.

In this experiment there were one 9-inch fuel plate holder, seven 3-inch fuel plate holders, and six 1-inch suppressor plate holders.

Figure 3 is a drawing of the nine-inch plate holder. This holder differs from the three-inch holder in two respects: (a) the sample fuel plate length is nominally nine inches instead of three inches and (b) the side plates of the nine-inch holder are extended by about 1-1/2 inches. The extended side plates rested upon the outer edge of the top of the lower end box forming a plenum to assure minimal restriction of flow through the outer coolant channels.

The sample fuel plates are supported at the bottom of each holder by a horizontal lip of the side plates and were not attached to the side plates. This arrangement permitted ready access to the fuel plates during post-irradiation examination although some structural integrity was sacrificed.

The one-inch holders were identical to the three-inch holders except for the difference in axial dimension as implied by the nomenclature. The 12 plates inserted in each of the holders contained 35 weight percent B_4C in a 0.040-inch thick 1100 aluminum core, clad with 0.005 inch of 1100 aluminum on both sides, but not on the edges. A one-inch holder was inserted at each end of the holders containing fuel plates to decrease the axial flux variation.

Some of the three-inch fuel plates did not satisfy the drawing dimensions in that the fuel core edge to plate edge dimension was found by radiography to be less than 7/32 inch, but always greater than 1/8 inch. The groove depth in the plate holder side plates was decreased by 0.060 inch to avoid the possibility of covering the fuel core with the side plate web since burnout heat flux had been found experimentally to decrease substantially if the channel corners were heated significantly.

1.2 Fuel Compositions

Tables V through X list the physical characteristics of the fuel sample plates. Core position 1 is the top position and is about 18 inches above the reactor centerline.

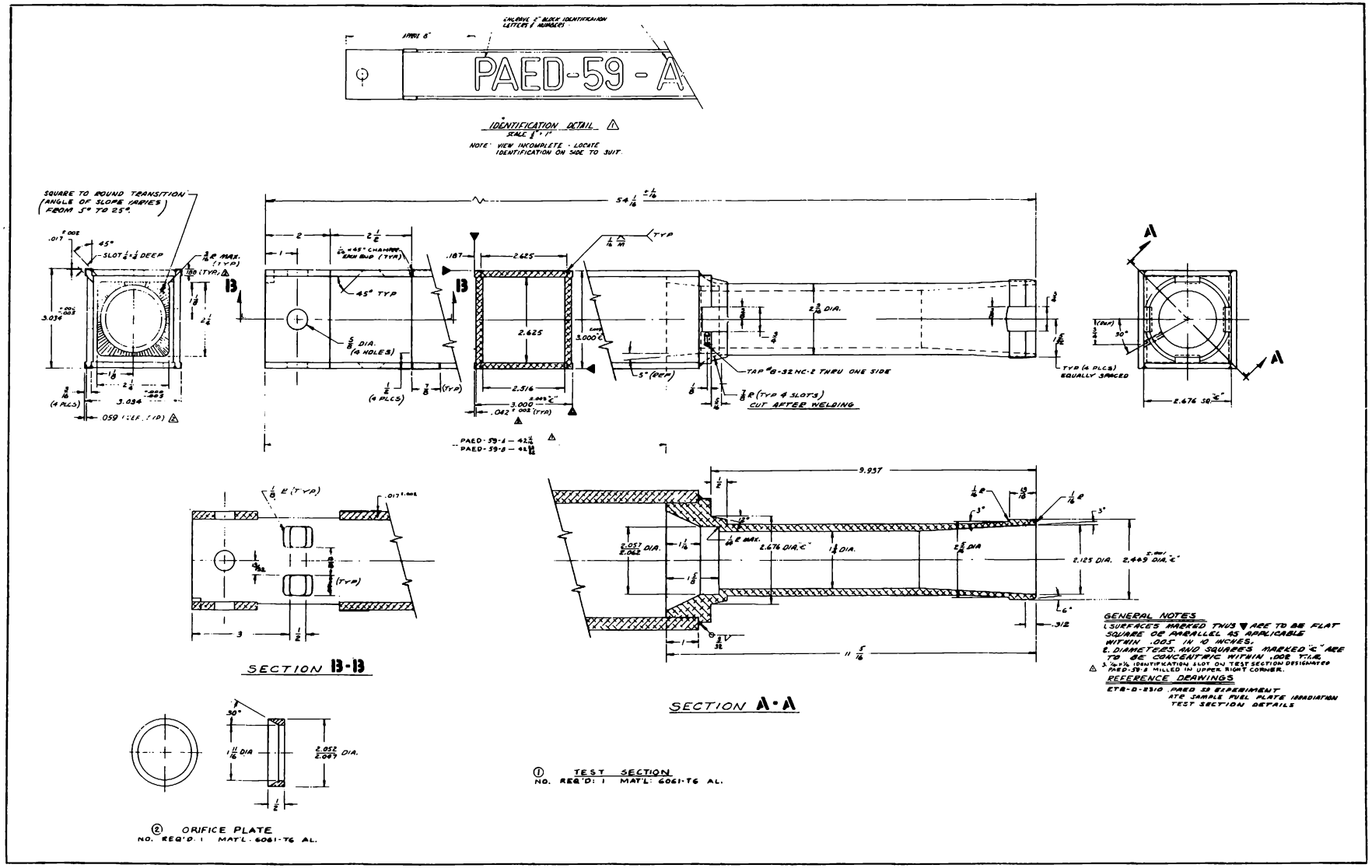

Fig. 2 PAED-59 experiment ATR sample fuel plate irradiation test section details.

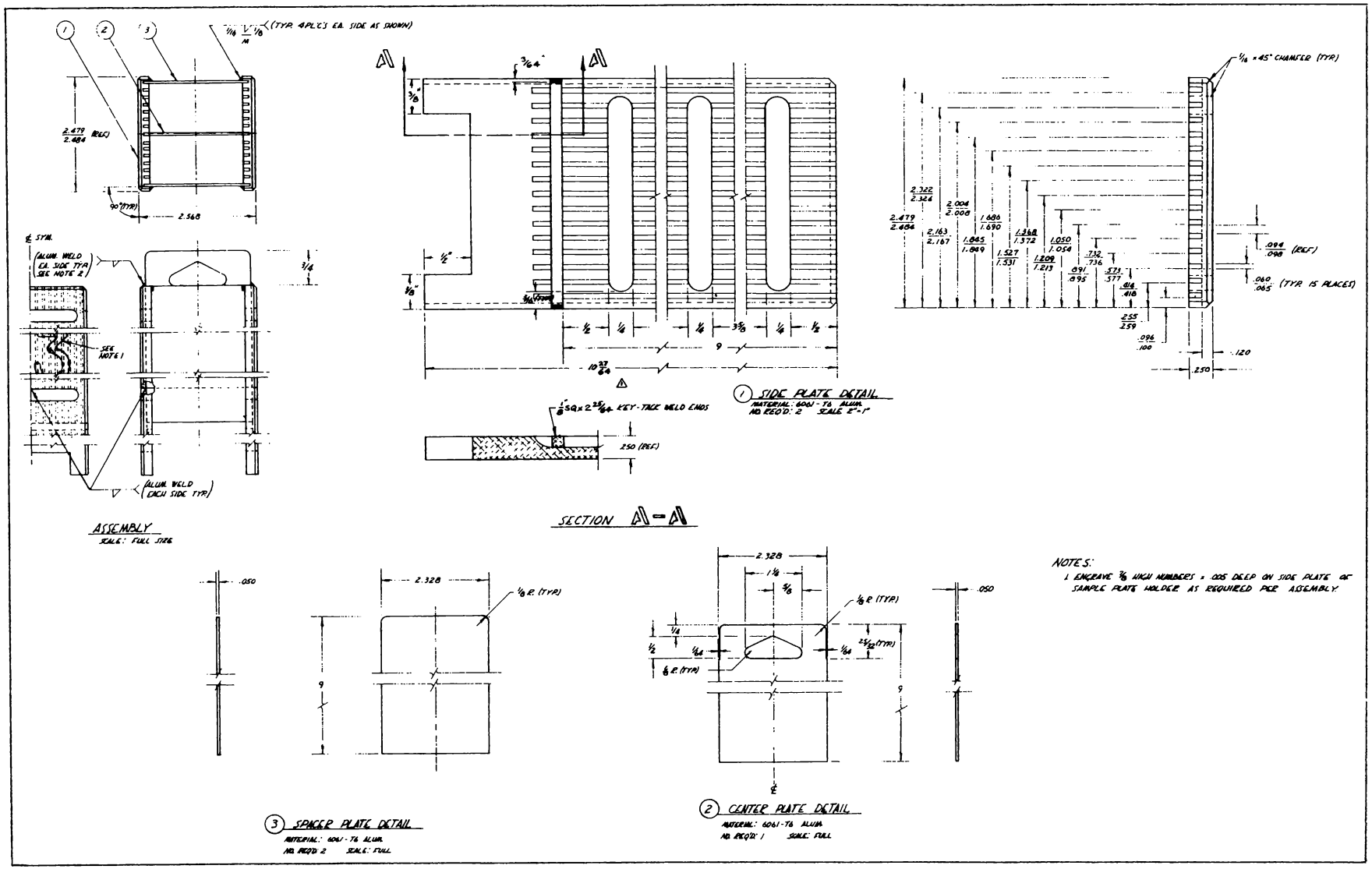

Fig. 3 PAED-59 experiment ATR sample fuel plate irradiation 9-inch fuel plate holder assembly and details.

TABLE V

CORE PIECE POSITION 3, HOLDER NUMBER 10

Plate Position	Plate No.	Composition No.	Total Wt (g)	Wt of Uranium (g)	Wt of U-235 (g)	Fuel Core Alloy	Cladding Material	Coating (in.)	Remarks
1	E-225	Blank Plate	15.128	None	None	None	6061-T6	None	--
2	E-49	ATR 2	15.769	1.425	1.325	32 wt% UO_2 in X-8001	X-8001 Al	0.0019	0.187 wt % B_4C in Fuel Core
3	E-50	ATR 2	15.737	1.428	1.329	32 wt% UO_2 in X-8001	X-8001 Al	0.0019	0.187 wt % B_4C in Fuel Core
4	E-51	ATR 2	15.750	1.435	1.335	32 wt% UO_2 in X-8001	X-8001 Al	0.002	0.187 wt % B_4C in Fuel Core
5	E-48	ATR 2	15.774	1.421	1.321	32 wt% UO_2 in X-8001	X-8001 Al	0.0019	0.187 wt % B_4C in Fuel Core
6	E-324	Blank Plate	14.128	None	None	None	6061-T6	None	--
7	E-239	Blank Plate	14.128	None	None	None	6061-T6	None	--
8	E-53	ATR 8	15.797	1.420	1.321	32 wt% UO_2 in X-8001	6061-0	0.0024	0.187 wt % B_4C in Fuel Core
9	E-55	ATR 8	15.626	1.418	1.319	32 wt% UO_2 in X-8001	6061-0	0.0024	0.187 wt % B_4C in Fuel Core
10	E-62	ATR 8	15.628	1.428	1.329	32 wt% UO_2 in X-8001	6061-0	0.0023	0.187 wt % B_4C in Fuel Core
11	E-59	ATR 8	15.845	1.423	1.324	32 wt% UO_2 in X-8001	6061-0	0.0023	0.187 wt % B_4C in Fuel Core
12	E-319	Flux Plate	15.428	None	None	None	6061-T6	None	Flux Monitor

TABLE VI

CORE PIECE POSITION 4, HOLDER NUMBER 19

Plate Position	Plate No.	Composition No.	Total Wt (g)	Wt of Uranium (g)	Wt of U-235 (g)	Fuel Core Alloy	Cladding Material	Coating (in.)	Remarks
1	E-311	Flux Plate	15.128	None	None	None	6061-T6 Al	None	Flux Monitor
2	E-9	ATR 1	15.1982	1.464	1.363	35 wt% U_3O_8 in X-8001	X-8001 Al	0.0020	0.19 wt% B_4C in Fuel Core
3	E-11	ATR 1	15.452	1.463	1.363	35 wt% U_3O_8 in X-8001	X-8001 Al	0.0022	0.19 wt% B_4C in Fuel Core
4	E-4	ATR 1	15.563	1.466	1.366	35 wt% U_3O_8 in X-8001	X-8001 Al	0.0019	0.19 wt% B_4C in Fuel Core
5	E-8	ATR 1	16.043	1.471	1.370	35 wt% U_3O_8 in X-8001	X-8001 Al	0.0017	0.19 wt% B_4C in Fuel Core
6	E-320	Flux Plate	15.128	None	None	None	6061-T6 Al	None	Flux Monitor
7	E-221	Blank Plate	15.128	None	None	None	6061-T6 Al	None	--
8	E-26	ATR 7	15.797	1.463	1.362	35 wt% U_3O_8 in X-8001	6061-0 Al	0.0023	0.19 wt% B_4C in Fuel Core
9	E-18	ATR 7	15.486	1.465	1.365	35 wt% U_3O_8 in X-8001	6061-0 Al	0.0023	0.19 wt% B_4C in Fuel Core
10	E-19	ATR 7	15.469	1.465	1.364	35 wt% U_3O_8 in X-8001	6061-0 Al	0.0020	0.19 wt% B_4C in Fuel Core
11	E-25	ATR 7	15.733	1.466	1.365	35 wt% U_3O_8 in X-8001	6061-0 Al	0.0023	0.19 wt% B_4C in Fuel Core
12	E-324	Flux Plate	15.128	None	None	None	6061-T6	None	Flux Monitor

TABLE VII

CORE PIECE POSITION 5, HOLDER NUMBER 21

Plate Position	Plate No.	Composition No.	Total Wt (g)	Wt of Uranium (g)	Wt of U-235 (g)	Fuel Core Alloy	Cladding Material	Coating (in.)	Remarks
1	E-318	Blank Plate	15.128	None	None	None	6061-T6	None	--
2	E-85	ATR 3	15.280	1.455	1.334	40 wt% UAl_3 in X-8001	X-8001 Al	0.0015	0.19 wt% B_4C in Fuel Core
3	E-80	ATR 3	14.903	1.450	1.330	40 wt% UAl_3 in X-8001	X-8001 Al	0.0015	0.19 wt% B_4C in Fuel Core
4	E-83	ATR 3	14.812	1.455	1.334	40 wt% UAl_3 in X-8001	X-8001 Al	0.0015	0.19 wt% B_4C in Fuel Core
5	E-490	ATR 3	15.232	1.480	1.357	40 wt% UAl_3 in X-8001	X-8001 Al	0.0015	0.19 wt% B_4C in Fuel Core
6	E-316	Blank Plate	15.128	None	None	None	6061-T6	None	--
7	E-229	Blank Plate	15.128	None	None	None	6061-T6	None	--
8	E-94	ATR 9	15.230	1.456	1.335	40 wt% UAl_3 in X-8001	6061-0 Al	0.0015	0.19 wt% B_4C in Fuel Core
9	E-99	ATR 9	15.586	1.447	1.327	40 wt% UAl_3 in X-8001	6061-0 Al	0.0015	0.19 wt% B_4C in Fuel Core
10	E-101	ATR 9	15.620	1.456	1.335	40 wt% UAl_3 in X-8001	6061-0 Al	0.0015	0.19 wt% B_4C in Fuel Core
11	E-102	ATR 9	15.532	1.456	1.335	40 wt% UAl_3 in X-8001	6061-0 Al	0.0015	0.19 wt% B_4C in Fuel Core
12	E-315	Blank Plate	15.128	None	None	None	6061-T6	None	--

TABLE VIII

CORE PIECE POSITION 6, HOLDER NUMBER 18

Plate Position	Plate No.	Composition No.	Total Wt (g)	Wt of Uranium (g)	Wt of U-235 (g)	Fuel Core Alloy	Cladding Material	Coating (in.)	Remarks
1	E-326	Flux Plate	15.128	None	None	None	6061-T6	None	Flux Monitor
2	E-240	Blank Plate	15.128	None	None	None	6061-T6	None	--
3	E-241	Blank Plate	15.128	None	None	None	6061-T6	None	--
4	E-520	ATR 6	15.795	1.971	1.834	41 wt% UO_2 in X-8001	6061-0 Al	0.0005	0.19 wt% B_4C in Fuel Core
5	E-515	ATR 6	16.110	1.976	1.838	41 wt% UO_2 in X-8001	6061-0 Al	0.0005	0.19 wt% B_4C in Fuel Core
6	E-314	Flux Plate	15.128	None	None	None	6061-T6	None	Flux Monitor
7	E-312	Flux Plate	15.128	None	None	None	6061-T6	None	Flux Monitor
8	E-518	ATR 6	16.002	1.973	1.836	41 wt% UO_2 in X-8001	6061-0 Al	0.0005	0.19 wt% B_4C in Fuel Core
9	E-519	ATR 6	15.906	1.974	1.836	41 wt% UO_2 in X-8001	6061-0 Al	0.0005	0.19 wt% B_4C in Fuel Core
10	E-236	Blank Plate	15.128	None	None	None	6061-T6	None	--
11	E-237	Blank Plate	15.128	None	None	None	6061-T6	None	--
12	E-323	Flux Plate	15.128	None	None	None	6061-T6	None	Flux Monitor

TABLE IX

CORE PIECE POSITION 7, HOLDER NUMBER 17

Plate Position	Plate No.	Composition No.	Total Wt (g)	Wt of Uranium (g)	Wt of U-235 (g)	Fuel Core Alloy	Cladding Material	Coating (in.)	Remarks
1	E-326	Flux Plate	15.128	None	None	None	6061-T6	None	Flux Monitor
2	E-28	ATR 5	15.376	1.997	1.859	44 wt% U_3O_8 in X-8001	6061-0 Al	0.00075	0.19 wt% B_4C in Fuel Core
3	E-31	ATR 5	15.787	1.990	1.854	44 wt% U_3O_8 in X-8001	6061-0 Al	0.00075	0.19 wt% B_4C in Fuel Core
4	E-33	ATR 5	15.272	2.000	1.862	44 wt% U_3O_8 in X-8001	6061-0 Al	0.00075	0.19 wt% B_4C in Fuel Core
5	E-38	ATR 5	16.197	2.001	1.864	44 wt% U_3O_8 in X-8001	6061-0 Al	0.00075	0.19 wt% B_4C in Fuel Core
6	E-306	Flux Plate	15.128	None	None	None	6061-T6	None	Flux Monitor
7	E-233	Flux Plate	15.128	None	None	None	6061-T6	None	--
8	E-107	ATR 4	15.197	1.946	1.784	54 wt% UAl_3 in X-8001	6061-0	0.00075	0.19 wt% B_4C in Fuel Core
9	E-508	ATR 4	16.130	1.969	1.805	54 wt% UAl_3 in X-8001	6061-0	0.00075	0.19 wt% B_4C in Fuel Core
10	E-510	ATR 4	16.221	1.970	1.806	54 wt% UAl_3 in X-8001	6061-0	0.00075	0.19 wt% B_4C in Fuel Core
11	E-507	ATR 4	16.169	1.957	1.794	54 wt% UAl_3 in X-8001	6061-0	0.00075	0.19 wt% B_4C in Fuel Core
12	E-310	Flux Plate	15.128	None	None	None	6061-T6	None	Flux Monitor

1.3 ETRC Measurements

Several different measurements of the perturbed thermal neutron flux and fission rates within an identical experimental piece were made in the ETR Critical Facility. The final set of measurements that was used in the heat transfer calculations and the fuel burnup calculations is shown graphically in Figure 4. The ETRC core at this time was a nuclear mock-up of the ETR core used during Cycle 54 and 55.

The ratios used to compute the fission rates for those plates where no measurements were made were as shown in Table XI.

To convert the measured fission rate per gram of U-235 to thermal neutron flux the former was multiplied by 0.606. This is not the same factor as would be applied if the fissions caused by neutrons having energies greater than thermal were not considered.

1.4 Hydraulic Measurements

The water flow rate through the experimental assembly was measured in the ETR Hydraulic Facility. The orifice inside diameter near the exit was established at 1-5/16 inches to give an average velocity of 27.5 fps in the channels formed by the fuel plates.

TABLE X

CORE PIECE POSITION 8, HOLDER NUMBER 92

Plate Position	Plate No.	Composition No.	Total Wt (g)	Wt of Uranium (g)	Wt of U-235 (g)	Fuel Core Alloy	Cladding Material	Coating (in.)	Remarks
1	E-339	Flux Plate	46.310	None	None	None	6061-T6 Al	None	Flux Monitor
2	E-117	ETR 10	48.218	2.697	2.522	22 wt% UAl in 1100 Al	1100 Al	None	--
3	E-124	ETR 10	47.3506	2.707	2.322	22 wt% UAl in 1100 Al	1100 Al	None	--
4	E-129	ETR 10	45.742	2.658	2.473	22 wt% UAl in 1100 Al	1100 Al	None	--
5	E-134	ETR 10	45.523	2.611	2.429	22 wt% UAl in 1100 Al	1100 Al	None	--
6	E-340	Flux Plate	46.310	None	None	None	6061-T6 Al	None	Flux Monitor
7	E-142	Blank Plate	46.451	2.740	2.512	35 wt% UAl_3 in 1100 Al	6061-T6 Al	None	--
8	E-146	ETR 11	46.759	2.747	2.518	35 wt% UAl_3 in 1100 Al	1100 Al	None	--
9	E-147	ETR 11	45.614	2.738	2.510	35 wt% UAl_3 in 1100 Al	1100 Al	None	--
10	E-148	ETR 11	45.474	2.756	2.527	35 wt% UAl_3 in 1100 Al	1100 Al	None	--
11	E-341	Flux Plate	46.310	None	None	None	6061-T6 Al	None	Flux Monitor
12A-G	E-149 thru E-150	Electrolyzed Samples	2.04 to 2.08	None	None	None	6061-T6 Al	None	Electrolyzed Samples
12H-N	E-173 thru E-179	Electrolyzed Samples	5.54 to 5.63	None	None	None	304 SS	None	Electrolyzed Samples

2. TEMPERATURE CALCULATIONS

Table XII summarizes the results of the calculations resulting from the ETRC measurements. The alumina-cladding interface temperatures were calculated using a thermal conductivity of 1.2 Btu/hr-ft-°F and the coating thickness as measured by the supplier. The value of thermal conductivity resulted from heat transfer experiments conducted at ORNL and by Phillips Petroleum Co., AED. All of the heat transfer data presented are for full ETR power of 175 MW without any U-235 burnup or increase in the alumina coating thickness.

To evaluate the applicability of the plate irradiation data it was necessary to calculate the oxide-aluminum interfacial temperature as the cycle progressed. The heat flux was computed from initial (prior to any burnup) measurements made in the ETRC and the fuel remaining at any given time. ETRC measurements indicated the effective flux (thermal plus some fraction of the epithermal) to be 1.107 times the thermal flux. This factor was used in computing total absorption and, thereby, the fraction of U-235 remaining at any given time. The effective flux was assumed to remain constant throughout the cycle. From the calculated power and the coolant velocity measured in the Hydraulic Facility prior to insertion of the experiment (27.5 ft/sec) the oxide surface temperature was computed using the modified Colburn Correlation.

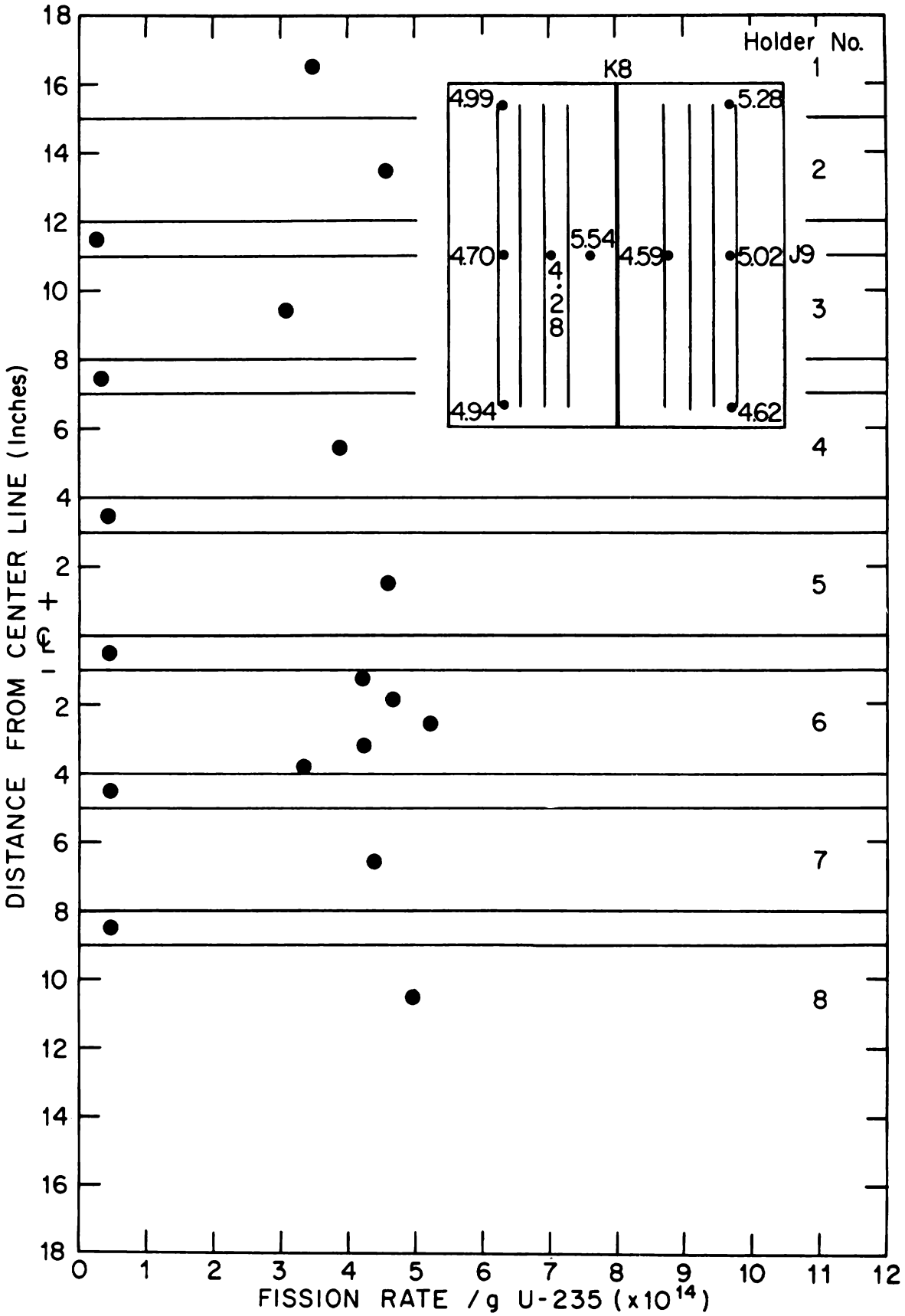

Fig. 4 Measurements used in heat transfer calculations.

TABLE XI

FISSION RATE RATIOS

Core Position	Plate Number	Maximum Ratio	Average Ratio
Three, Four, and Five	2	1.087	1.024
	3	1.034	0.974
	4	0.974	0.922
	5	1.131	1.065
	8	1.052	1.000
	9	1.084	1.031
	10	1.116	1.061
	11	1.150	1.094
Six	4	1.087	1.024
	5	1.087	1.024
	8	1.050	1.000
	9	1.150	1.092

The oxide thickness was computed from the Oak Ridge data [4]. The test with a specimen anodized to an assumed 0.3 mil (there is doubt about this dimension because of the anodizing technique employed) showed the rate of oxide buildup to be the same as bare surfaces. The tests with 2.00 and 2.84 mils of initial oxide coating were inconclusive. The 2.84 mils coated 6061 specimen was tested for only five days and showed a reduction in thickness of approximately 0.2 mil. The 2.00 mil clad X-8001 specimen showed an increase in oxide thickness (or at least temperature) with time but at a slower rate than bare surfaces. There is insufficient data available to separate the effect of the transition of the anodized surface to boehmite from the buildup of additional oxide or to indicate the effect of irradiation on the thermal conductivity of oxide-boehmite coating (exploratory tests indicate a reduction in thermal conductivity with irradiation).

Because of the above uncertainties, considerable engineering judgment was used to determine the temperature drop across the coating. The oxide was assumed to increase in thickness at the same rate as bare aluminum surfaces exposed at a pH of 5.7 to 7.0 ($X = 1200 \frac{\theta^{0.728}}{e^{\frac{8290}{^\circ R}}}$). This increase was assumed to continue until the thickness built up to the maximum value measured at the termination of the experiment and then to remain constant (in several instances the computed thickness never reached the maximum measured value). The thermal conductivity of the coating was assumed to remain constant at 1.2 Btu/hr-ft-°F.

TABLE XII

ATR FUEL IRRADIATION IN J-8, ETR t_{in} = 43°C, V = 27.5 fps

Core Holder Position	Plate Position	Plate No.	Composition No.	Avg Thermal Neutron Flux x 10^{14}	Max q/A Btu/hr-ft^2 x 10^6	Avg q/A Btu/hr-ft^2 x 10^6	$t_{w,max}$ °C	t_w @ °C	$t_{if,max}$ (a) °C	t_{if} @ (a) °C
3	2	E-49	ATR-2	1.87	0.67	0.63	96	93	144	139
	3	E-50	ATR-2	1.78	0.64	0.60	94	91	141	136
	4	E-51	ATR-2	1.68	0.61	0.58	92	89	138	133
	5	E-48	ATR-2	1.95	0.70	0.66	97	94	148	142
3	8	E-53	ATR-8	1.82	0.65	0.62	94	92	154	149
	9	E-55	ATR-8	1.88	0.67	0.63	96	93	157	152
	10	E-62	ATR-8	1.93	0.69	0.66	98	94	163	152
	11	E-59	ATR-8	1.99	0.71	0.68	98	96	161	156
4	2	E-9	ATR-1	2.40	0.89	0.84	111	107	180	171
	3	E-11	ATR-1	2.29	0.85	0.80	108	104	178	172
	4	E-4	ATR-1	2.17	0.80	0.76	106	102	164	157
	5	E-8	ATR-1	2.50	0.93	0.88	114	109	175	167
4	8	E-26	ATR-7	2.35	0.85	0.81	109	105	185	177
	9	E-18	ATR-7	2.42	0.89	0.84	111	107	190	181
	10	E-19	ATR-7	2.50	0.92	0.87	114	110	185	177
	11	E-25	ATR-7	2.57	0.94	0.89	115	111	199	190
5	2	E-85	ATR-3	2.85	1.03	0.97	122	117	182	173
	3	E-80	ATR-3	2.71	0.98	0.92	118	114	175	167
	4	E-83	ATR-3	2.56	0.92	0.88	111	112	166	163
	5	E-490	ATR-3	2.96	1.09	1.03	126	121	188	180
5	8	E-94	ATR-9	2.78	0.98	0.95	121	116	179	171
	9	E-99	ATR-9	2.87	1.02	0.97	122	117	181	173
	10	E-101	ATR-9	2.95	1.06	1.01	124	119	185	178
	11	E-102	ATR-9	3.04	1.10	1.04	126	122	188	182
6	4	E-520	ATR-6	3.22	1.61	1.51	157	150	188	179
	5	E-515	ATR-6	3.22	1.61	1.52	157	150	188	179
	8	E-518	ATR-6	3.15	1.56	1.48	154	149	184	177
	9	E-519	ATR-6	3.15	1.56	1.48	154	149	184	177
7	2	E-28	ATR-5	2.68	1.36	1.27	143	137	182	174
	3	E-31	ATR-5	2.55	1.29	1.21	139	133	176	168
	4	E-33	ATR-5	2.41	1.22	1.15	139	135	174	168
	5	E-38	ATR-5	2.79	1.41	1.33	151	144	192	178
7	8	E-107	ATR-4	2.62	1.26	1.20	142	137	178	172
	9	E-508	ATR-4	2.70	1.31	1.25	145	140	183	176
	10	E-510	ATR-4	2.78	1.35	1.29	144	138	183	176
	11	E-507	ATR-4	2.87	1.39	1.32	146	140	186	178
8	2	E-117	ETR-10	2.99	0.75	0.6	113	102	None	None
	3	E-124	ETR-10	2.99	0.75	0.6	113	102	None	None
	4	E-129	ETR-10	2.99	0.75	0.6	113	102	None	None
	5	E-134	ETR-10	2.99	0.75	0.6	113	102	None	None
8	7	E-142	ETR-11	2.99	0.75	0.6	113	102	None	None
	8	E-146	ETR-11	2.99	0.75	0.6	113	102	None	None
	9	E-147	ETR-11	2.99	0.75	0.6	113	102	None	None
	10	E-148	ETR-11	2.99	0.75	0.6	113	102	None	None

(a) Thermal conductivity of alumina ± 1.2 Btu/hr-ft, °F.

The results of the calculations of the centerline interface temperature as a function of full power operating time are shown for the five fuel compositions of interest in Figures 5 through 9, and are summarized in the following table:

Composition	Centerline calculated interface temperature, °C
32 Wt% UO_2	154
35 Wt% U_3O_8	178
40 Wt% UAl_3	180
41 Wt% UO_2	218
54 Wt% UAl_3 or 44 Wt% U_3O_8	206

For those plates where the calculated film thickness did not obtain maximum measured alumina coating thickness, the interface temperature for the latter thickness was calculated and is shown on the appropriate figure.

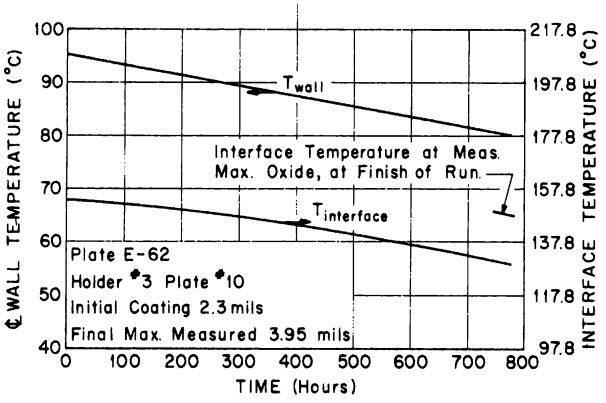

Fig. 5 Calculated coating-clad interface temperature for plate E-62.

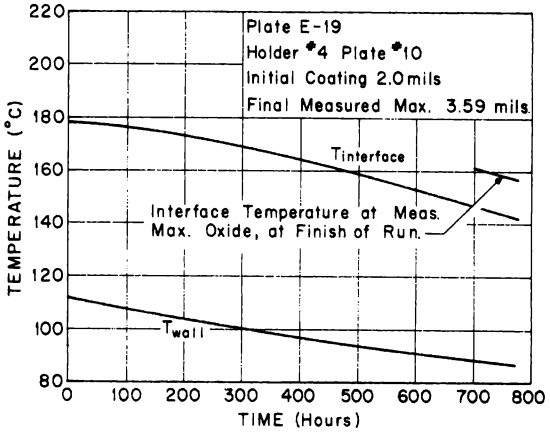

Fig. 6 Calculated coating-clad interface temperature for plate E-19.

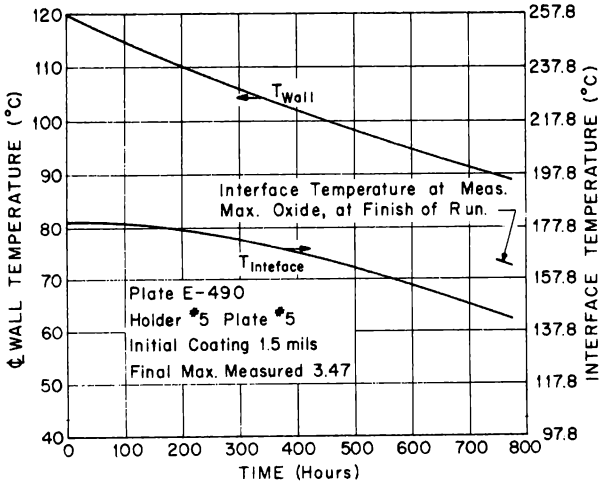

Fig. 7 Calculated coating-clad interface temperature for plate E-490.

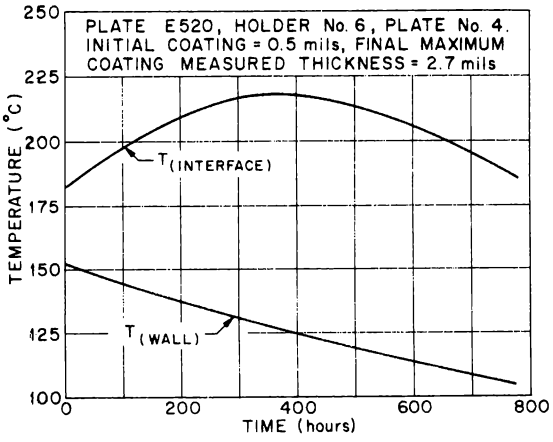

Fig. 8 Calculated coating-clad interface temperature for plate E-520.

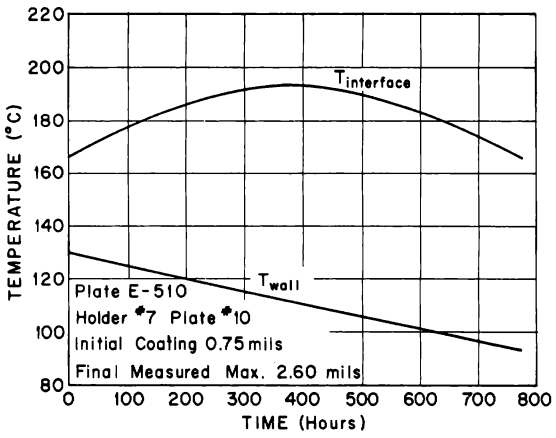

Fig. 9 Calculated coating-clad interface temperature for plate E-510.

3. FUEL BURNUP MEASUREMENTS AND CALCULATIONS

Chemical analyses of one plate from each of the five compositions were conducted to determine the U-235 burnup. Three different methods were used with essential agreement among the three.

Fuel burnup was calculated assuming a constant effective flux as determined by ETRC fission rate measurements and a total cross section of 680 barns. These calculations are compared with the measured values:

Composition	Measured Burnup, % Original U-235	Calculated Burnup, % Original U-235
32 Wt% UO_2	29	30
35 Wt% U_3O_8	33	37
40 Wt% UAl_3	39	41
44 Wt% U_3O_8	37	38
54 Wt% UAl_3	37	38

The calculations of heat flux, both initially and as the irradiation progressed, are substantiated by the reasonably good agreement shown in the comparison of measured and calculated fuel burnup.

The calculated fission densities, using the corrected neutron flux values, are shown in Table XIII. It was assumed in these calculations that the neutron flux was constant during the irradiation.

TABLE XIII

CALCULATED FISSION DENSITIES

Plate Identification	Composition (wt%)	Corrected Avg nvt x 10^{20} (n/cm2)	Corrected $e^{-\sigma_f \Phi \Delta t}$	Avg Fissions/ cc x 10^{20}
E-49	32 UO_2	5.8	0.72	5.9
E-50	32 UO_2	3.1	0.84	3.4
E-51	32 UO_2	5.2	0.73	5.6
E-48	32 UO_2	6.0	0.71	6.0
E-53	32 UO_2	5.6	0.72	5.7
E-55	32 UO_2	5.8	0.72	5.7
E-62	32 UO_2	6.0	0.71	6.1
E-59	32 UO_2	6.1	0.70	6.1
E-9	35 U_3O_8	7.4	0.65	7.4
E-11	35 U_3O_8	7.1	0.66	7.1
E-4	35 U_3O_8	6.7	0.68	6.8
E-8	35 U_3O_8	7.7	0.64	7.7
E-26	35 U_3O_8	7.2	0.66	7.3
E-18	35 U_3O_8	7.4	0.65	7.5
E-19	35 U_3O_8	7.7	0.64	7.7
E-25	35 U_3O_8	7.9	0.63	7.8
E-85	40 UAl_3	8.8	0.60	8.3
E-80	40 UAl_3	8.3	0.62	7.9
E-83	40 UAl_3	7.9	0.63	7.6
E-490	40 UAl_3	9.0	0.59	8.6
E-94	40 UAl_3	8.6	0.61	8.2
E-99	40 UAl_3	8.8	0.60	8.3
E-101	40 UAl_3	5.1	0.74	5.3
E-102	40 UAl_3	9.4	0.58	8.7
E-520	41 UO_2	9.9	0.56	12.5
E-515	41 UO_2	9.9	0.56	12.5
E-518	41 UO_2	9.7	0.57	12.3
E-519	41 UO_2	9.7	0.57	12.3
E-28	44 U_3O_8	8.3	0.62	11.0
E-31	44 U_3O_8	4.4	0.78	6.5
E-33	44 U_3O_8	7.4	0.65	10.2
E-38	44 U_3O_8	8.6	0.61	11.4
E-107	54 UAl_3	8.1	0.63	10.4
E-508	54 UAl_3	8.3	0.62	10.7
E-510	54 UAl_3	8.6	0.61	11.0
E-507	54 UAl_3	8.8	0.60	11.2
E-12	35 U_3O_8	2.4	0.87	2.8
E-13	35 U_3O_8	3.5	0.82	3.9

IV. PLATE EXAMINATION

1. PRE-IRRADIATION INSPECTION

After fabrication, the sample fuel plates were subjected to a series of tests designed to determine their suitability for irradiation in the ETR, and to establish their metallurgical properties prior to irradiation so that the irradiation effects could be evaluated. The following properties of the fuel plates were measured: dimensions, weight, uniformity of fuel distribution in the core, location of the core, tendency for blister formation in the cladding, hardness of the core and cladding, thickness of the cladding, thickness of anodized coating, the quality of the bonds between the core, and the cladding and the density of the plates. In order to measure these properties, the following tests were performed:

(1) Blister Test - This was done by holding the plates at 590°C for one hour before the final cold rolling pass.

(2) Visual Inspection - This test was performed on the fuel plates before and after anodizing.

(3) Dimensional Check - The dimensions of the fuel plates were checked with a micrometer and a vernier caliper before and after anodizing.

(4) Gross Weight - The samples were weighed on an analytical balance before and after anodizing.

(5) Density Determination - This test was done by water immersion before and after the samples were anodized.

(6) Fluorescent Penetration - A Zyglo test was performed to inspect for pits and cracks.

(7) Whole Plate Alpha Counting - The samples were alpha counted on both sides before anodizing to insure that no uranium had diffused through the cladding during fabrication.

(8) Ultrasonic Inspection - The samples were inspected by immersion testing, using the through-transmission technique. Five MC Li_2SO_4 crystals were used with suitable standards to insure that nonbonds 1/8 inch in diameter or larger could be detected.

(9) Liquid Nitrogen Testing - The samples were submerged in liquid nitrogen until bubbling stopped. They were then quickly transferred to a bath of ethyl alcohol. Any crack would have been revealed by a stream of bubbles.

(10) Coating Thickness Measurement - The anodized coating thickness was measured by Sylcor using a Dermitron eddy-current instrument.

(11) Radiography - The samples were radiographed in order to determine the core location and fuel distribution. The following conditions were used: 66 inches source to plate, 75 kVp, type-M film, and 20 milliamp minutes.

(12) Metallography - One plate from each composition was cut up and prepared for metallographic examination. The purposes of this examination were to check the quality of the bonds between the cladding and core, to determine the thickness of the core and claddings, and to ascertain the uniformity of the fuel distribution in the cores. Photomicrographs were taken and microhardness measurements were made of the constituents for comparison with the post-irradiation microstructure and hardness.

2. POST-IRRADIATION EXAMINATION

The post-irradiation examination consisted of determining fuel plate physical and mechanical properties, metallography, qualitative analysis of oxide coatings and microconstituents, U-235 burnup analysis, and quantitative analysis of the fission gases collected from blisters. A flow sheet, Figure 10, shows how many samples were used for each step. The data were taken at the ETR canal, the MTR-ETR, TAN and AREA hot cells, and ICPP analytical laboratory.

The physical properties taken include a record of the plate appearance (ie, black and white and color photographs), weight before and after oxide film stripping, coating thickness measurements, dimensional surveys of plates before and after film stripping, dimensional surveys of blistered areas, and density determinations before and after film stripping.

Mechanical tests included microhardness of microconstituents and tensile tests at room temperature, and 204°C of all compositions except those that blistered.

Metallography was performed on specimens representative of each composition and for each thickness of aluminum oxide coating. Specimens were cut from the edge of the plate, the center of the plate, and those areas containing blisters.

Samples of coatings representing the spalled and the nonspalled surface conditions were analyzed qualitatively; likewise, each type core material was analyzed by hot X-ray diffraction. Burnup analysis was performed on one plate from each holder. The fission gas was collected from the blister of two of the uranium-oxide plates and analyzed for total gas content and mole percent of each gas present.

The examination involved over 600 photographs and photomicrographs, 34 metallographic mounts, over 600 hardness readings, over 600 thickness measurements, and over 400 length and width measurements. Since the data, filling more than nine laboratory notebooks, are so voluminous, it is reported here in condensed form in the following sections.

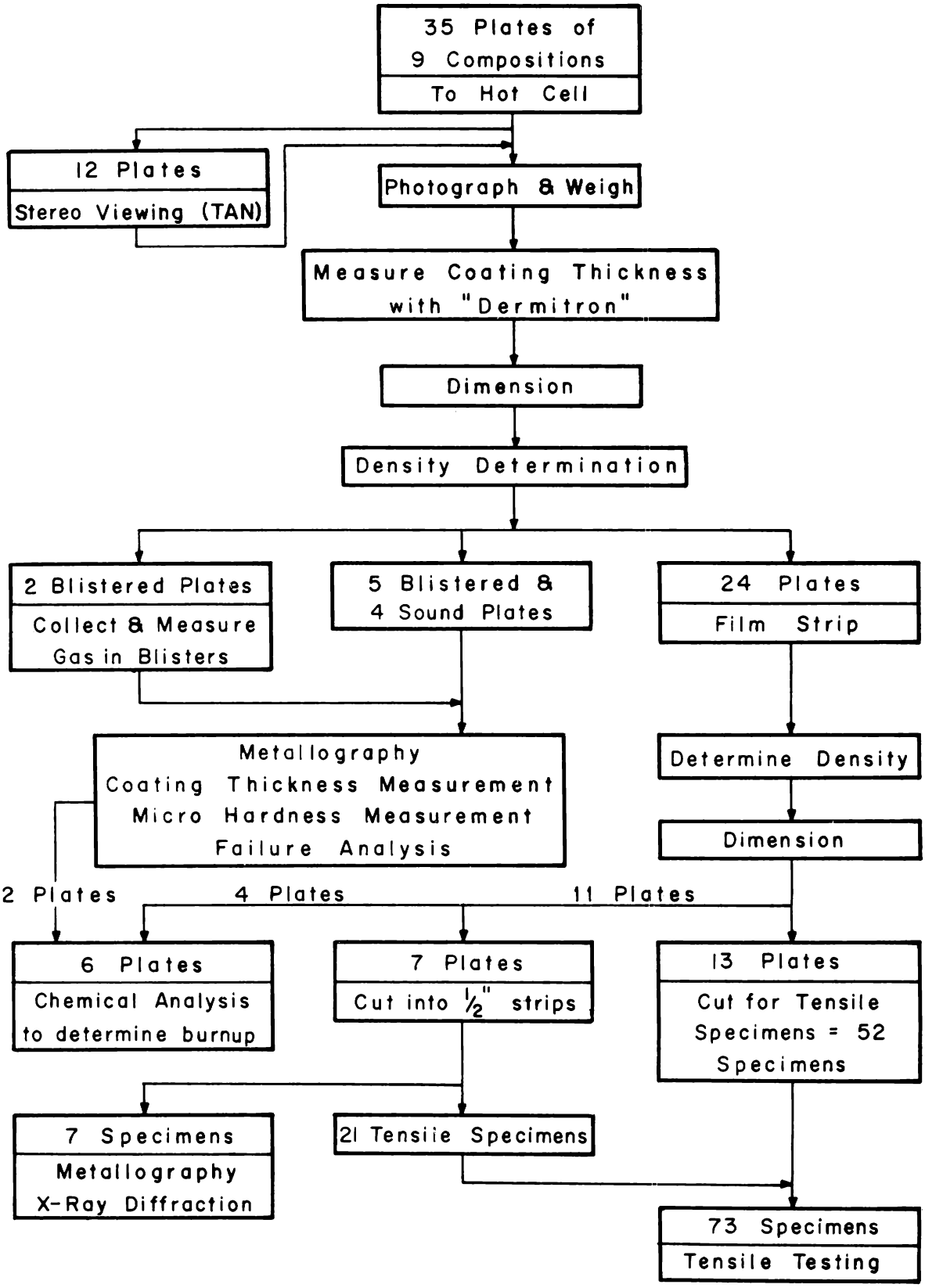

Fig. 10 Flowsheet of hot cell examination of ATR fuel irradiation samples.

V. EVALUATION AND SUMMARY OF TEST RESULTS

1. ALUMINUM OXIDE COATINGS

As discussed in Section II, the fuel plates were coated, by anodizing, with aluminum oxide to provide an insulating layer thereby increasing the temperature to simulate ATR conditions. The anodized coating was amorphous, had a density of 2.9 to 3.0, and varied (from plate to plate) in thickness from 0.5 mil to 2.3 mils depending on a particular type irradiation position in the reactor.

After irradiation and exposure to reactor cooling water the films exhibited three general surface appearances--nonspalled, partially spalled over the entire area of the core, and partially spalled over part of the core area leaving islands of nonspalled coating (Figures 11, 12, and 13). The partially spalled portions were found to contain boehmite while the nonspalled portions exhibited boehmite and small quantities of bayerite.

The coatings increased in thickness from 1.5 to 2 times the starting thickness during irradiation; the final densities ranged from 2.5 to 2.7.

Metallography shows that coatings vary from plate to plate and within a particular plate as to the number of layers present (Figure 14). There may be one layer, two layers, or three layers present in a given plate which vary in thickness. There was good correlation, however, between maximum thicknesses as determined by metallography and Dermitron readings, and also for thicknesses increases of plates with similar fuel type and content.

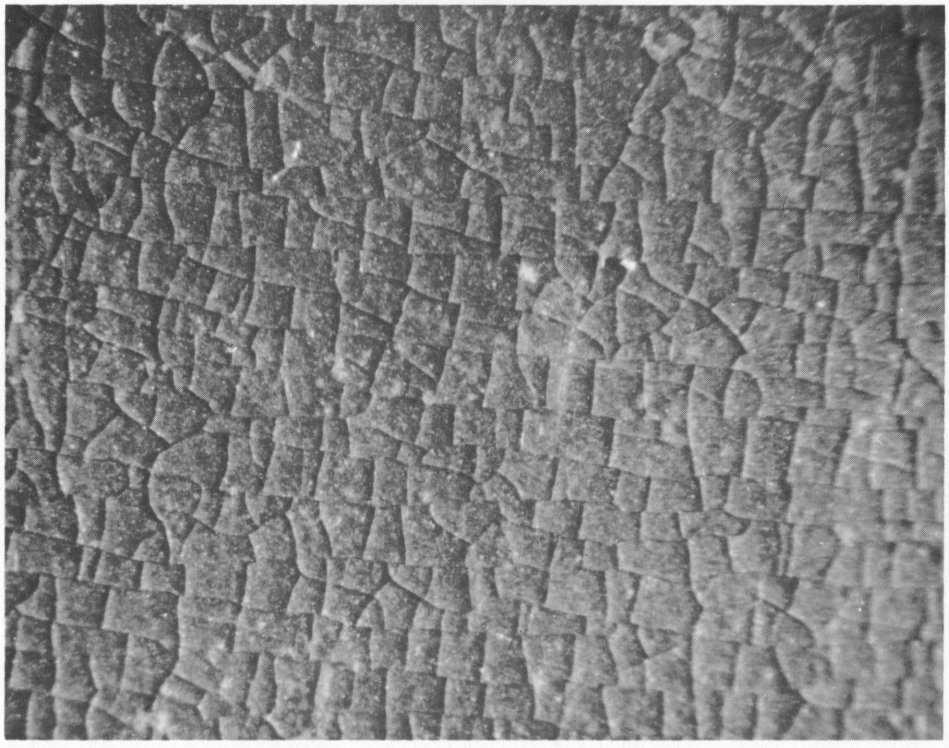

30X

Fig. 11 Aluminum oxide film after irradiation. This nonspalled type contained boehmite and bayerite.

30X

Fig. 12 Aluminum oxide film after irradiation. Although spalling took place, the coatings increased in thickness. A boehmite structure was detected.

30X

Fig. 13 Aluminum oxide film after irradiation exhibiting spalled and nonspalled areas.

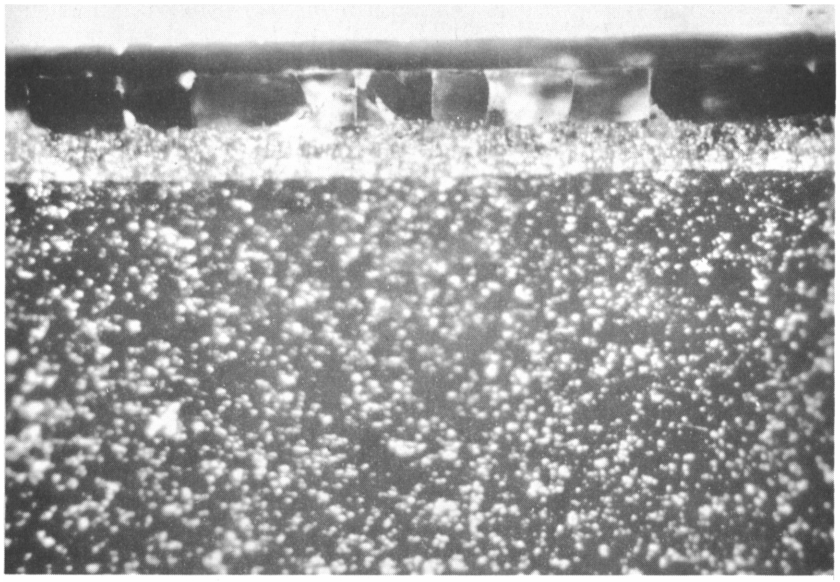

AS POLISHED 250X

COATED X-8001

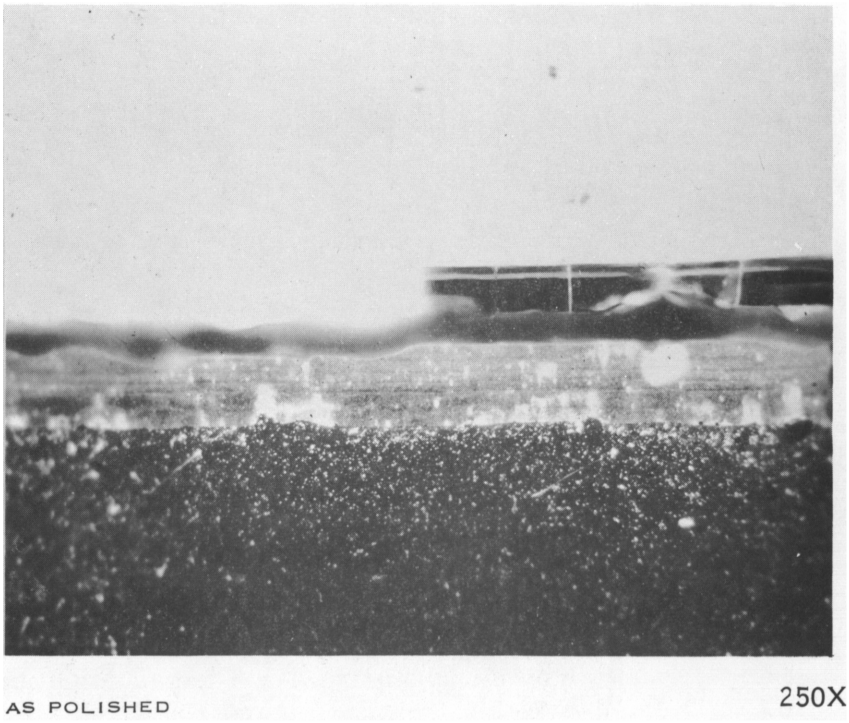

AS POLISHED 250X

COATED 6061

Fig. 14 Aluminum oxide coatings after irradiation.

The examinations and measurements made on oxide films did not resolve the unexpected complexities that affect heat transfer properties. Some of the complexities are the rate at which the oxide film builds up on an anodized coating of a certain starting thickness, thermal conductivity of the various composite layers, how conductivity of each layer is affected by neutron flux, the maximum thickness to which coatings build up on a particular plate type before spalling, and the effects of an irregular surface.

Whether these complexities could ever be resolved so that accurate, reliable temperatures could be determined by this method is questionable. It is clear, however, that coatings remained on the surface of the plates, after irradiation, that temperatures were significantly increased, and that a comparative performance test of the three fuel materials has been achieved.

2. FAILURE ANALYSIS OF BLISTERED PLATES

It has been anticipated for some time that uranium oxide fuel dispersions in aluminum had an upper limit of fuel loading, particularly when operated at elevated temperatures, because of the diffusion reaction between the fuel particles and the aluminum matrix. Even in stainless steel UO_2 dispersion fuels where no chemical reaction occurs, it has been shown that such a limit exists [5]. Studies of this instability have been reported in previous progress reports of the Reactor Fuels and Materials Development Program at MTR-ETR [6, 7]. It was not known, however, that this series of test plates would reach that upper limit or exactly how the fuel instability would contribute to failure. The following analyses of examination and test results describe how fuel instability and subsequent large void formation lead to blistering.

2.1 Visual Observation

After irradiation the fuel plates were examined visually. All of the 44 weight percent U_3O_8 plates and all of the 41 weight percent UO_2 plates that were irradiated for the full cycle had developed blisters (Figures 15 and 16). The 54 weight percent UAl_3 compositions, having an equal U-235 content, did not blister, nor did any of the lower weight percent compositions. Some of the uranium oxide plates had one blister, some had dual blisters, and one warped and developed multiple blisters. Blisters could be seen protruding an equal amount on both sides of the plates, suggesting core failure.

2.2 Fission Gas Analysis

The gas was collected from the blister of two plates (one UO_2 plate and one U_3O_8 plate) and analyzed for total quantity of gas and the gas composition (Table XIV). It was found that irradiation produced gases were present in sufficient quantities to cause a blister. Since the plate temperature was questionable, a pressure-temperature plot was made by two methods (one based on the perfect gas law and the other based on the yield strength of the cladding in conjunction with the maximum stress formula for thin shells with fixed edges [8]) to show, at the point where the curves cross, the approximate gas conditions at the time of blister formation. This is observed in Figure 17. The gas conditions for the formation of the UO_2 blister were 20 atmospheres and 230°C. This relation did not hold for the U_3O_8 blister because more irradiation-produced gas was collected than was required to form the blister. This was explained when metallography showed a split in the core adjoining the blister.

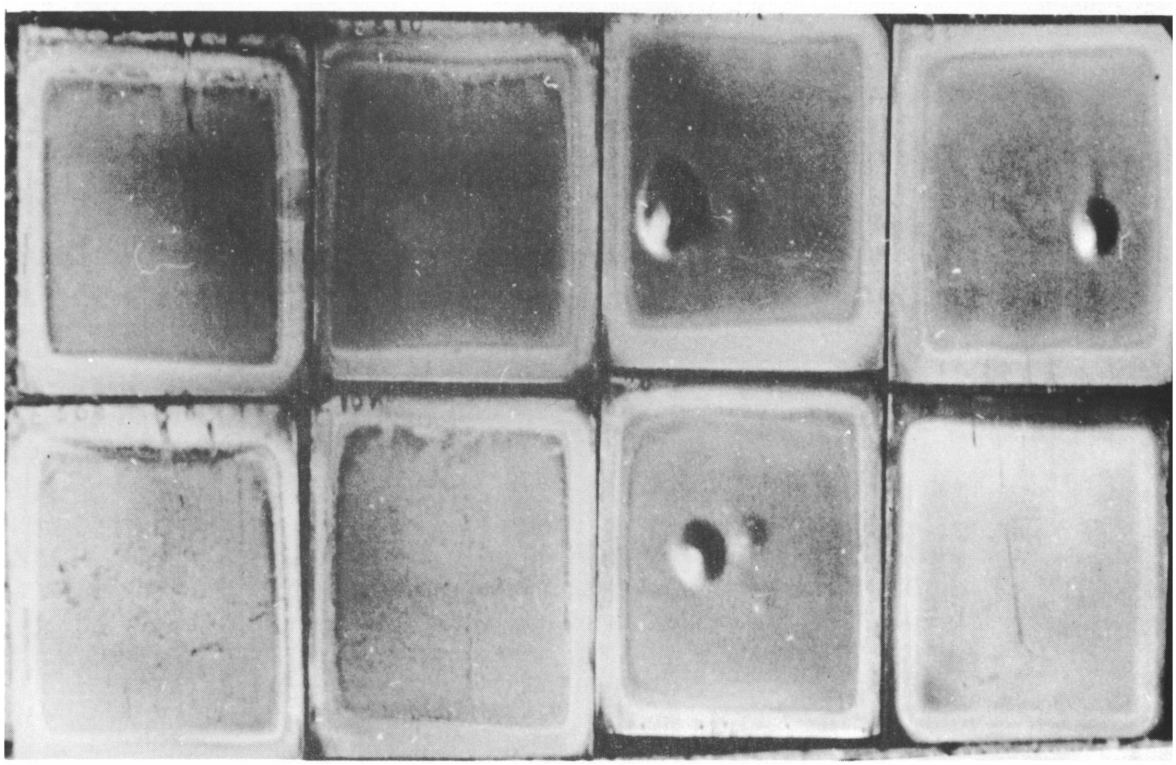

PLATES: 107, 507, 508 AND 510 ARE 54 WEIGHT PERCENT UAL_3 + X-8001 CORE CLAD WITH 6061, IRRADIATED TO 10.0 X 10^{20} FISSIONS/CC

PLATES: 28, 33 AND 38 ARE 44 WEIGHT PERCENT U_3O_8 + 8001 CORE CLAD WITH 6061, IRRADIATED TO 10.0 X 10^{20} FISSIONS/CC

PLATE: 13 IS A 35 WEIGHT PERCENT U_3O_8 + X-8001 CORE CLAD WITH X-8001, IRRADIATED TO 3.5 X 10^{20} FISSIONS/CC

Fig. 15 Plates irradiated in core position 7. All the 44 weight percent U_3O_8 plates blistered.

The gases collected from the blisters were primarily Xe, Kr, and He with only traces of H_2 and Ar. Small quantities of air found in the collection system were discounted because of a constant leak rate through the seals. Table XV shows the relative plate areas which produced the various fission gases collected. These ratios are the result of numerous complexities such as the rate of gas production (which changes with burnup); the relative rates of gas diffusion through the reacted particles (which are changing in composition) and through the aluminum matrix (which is changing in volume percent); and the time at which the blister nucleated in relation to fuel or poison burnup, temperature, pressure, and concentration of dissolved gases and strength of the material (which changes with radiation hardening, temperature, over-aging and annealing of radiation hardening).

The fact that He diffused into the blister from a greater distance than Xe and Kr (Table XV) can be explained by comparing the diffusion coefficients of He through Al (in the order of 10^{-10} cm^2/sec [9]) with the diffusion coefficients

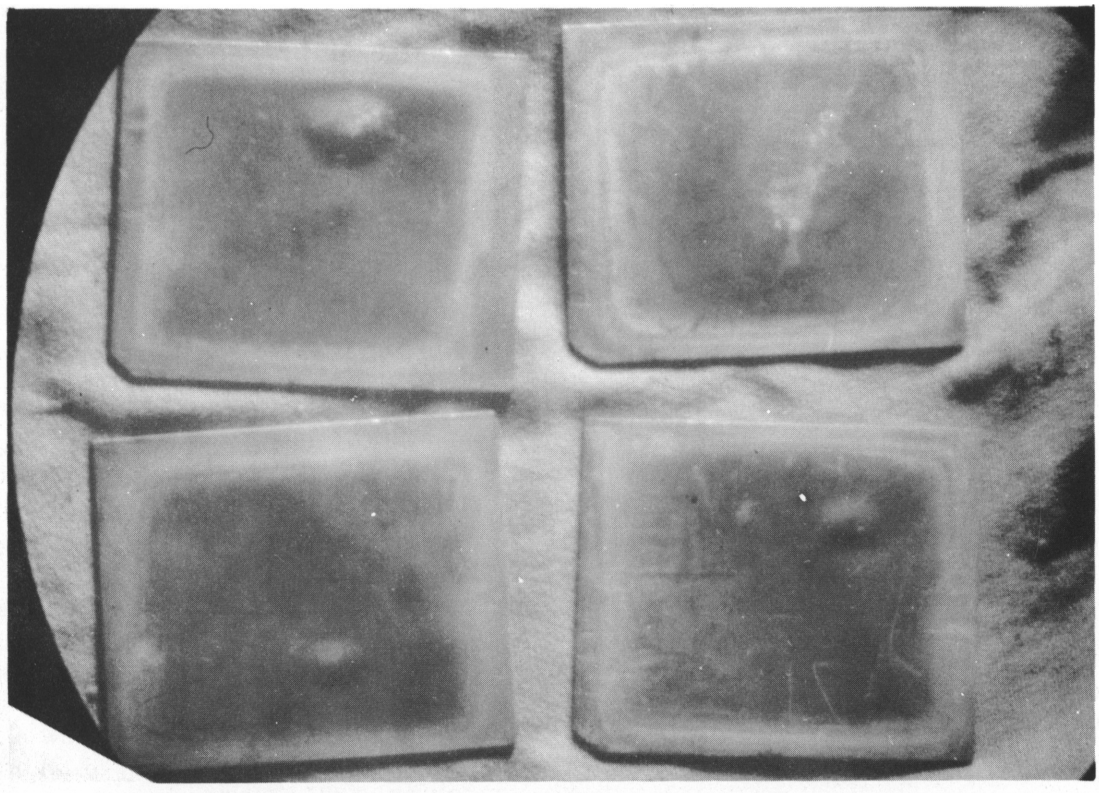

≈ 3/4X

Fig. 16 Photograph showing blistered UO_2 plates. All the 41 weight percent UO_2 plates blistered.

TABLE XIV

FISSION GASES COLLECTED FROM BLISTERED PLATES

	44 wt% U_3O_8 Plate	42 wt% UO_2 Plate
Volume of gas (STP)	1.79 cc	0.49 cc
Mole %... H_2	<0.1	0.4
He	19.5	41.2
N_2	1.7	8.9
O_2	<0.1	1.1
Ar	0.03	0.12
Kr	10.5	6.92
Xe	68.2	41.4

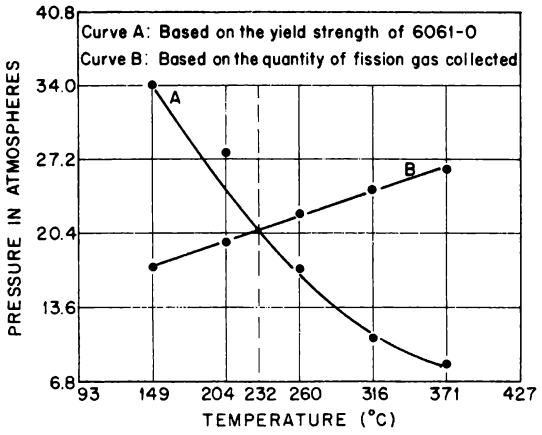

Fig. 17 Pressure in blister vs temperature by two methods for the 42 weight percent UO_2 plate.

of Xe and Kr through the oxides (10^{-18} through UO_2 and 10^{-15} through U_3O_8[10]). Likewise, Xe and Kr diffuse through U_3O_8 more readily than through UO_2 accounting for a higher percentage of these gases in the U_3O_8 blister (Table XIV).

2.3 Mechanisms of Blister Formation

It has been recognized and reported previously [6, 7] that a diffusion reaction, the rate of which is dependent on time, temperature, and irradiation, takes place between the uranium oxides and the aluminum matrix in these dispersion-type plates. Selected photomicrographs from this previous work show how these variables combine to produce totally reacted fuel particles. Figure 18 shows it is possible to produce a particle-matrix diffusion reaction out-of-pile simply by heating; but, the temperatures required are much higher (590°C) than plate temperatures needed for reactions produced in-pile. Similar results also have been reported by others [11, 12]. Figure 19 shows that significant reaction takes place at temperatures as low as 93°C in-pile with sufficiently high burnup. But, Figure 20 shows a totally reacted particle produced with low burnup and at a temperature (204°C) much lower than that required to produce diffusion out-of-pile. These reactions were observed in the U_3O_8 fuel plates (Figure 21) as well as in the UO_2; however, it takes longer for the U_3O_8 reaction to go to completion.

The reaction itself has not caused failure in plates with lower fuel loadings. But, in evaluating the 32 weight percent UO_2 core microstructures of the ATR

TABLE XV

RELATIVE AREAS OF PLATE REQUIRED TO PRODUCE FISSION GASES RECOVERED FROM BLISTERS

	41 wt% UO_2 Plate	44 wt% U_3O_8 Plate
Area of Blister	0.123 $in.^2$	0.292 $in.^2$
Ratio to Blistered Area	1.0	1.0
Area Required to Produce Xe	0.077 $in.^2$	0.494 $in.^2$
Ratio to Blistered Area	0.63	1.70
Area Required to Produce Kr	0.044 $in.^2$	0.265 $in.^2$
Ratio to Blistered Area	0.36	0.91
Area Required to Produce He	0.280 $in.^2$	0.500 $in.^2$
Ratio to Blistered Area	2.30	1.71

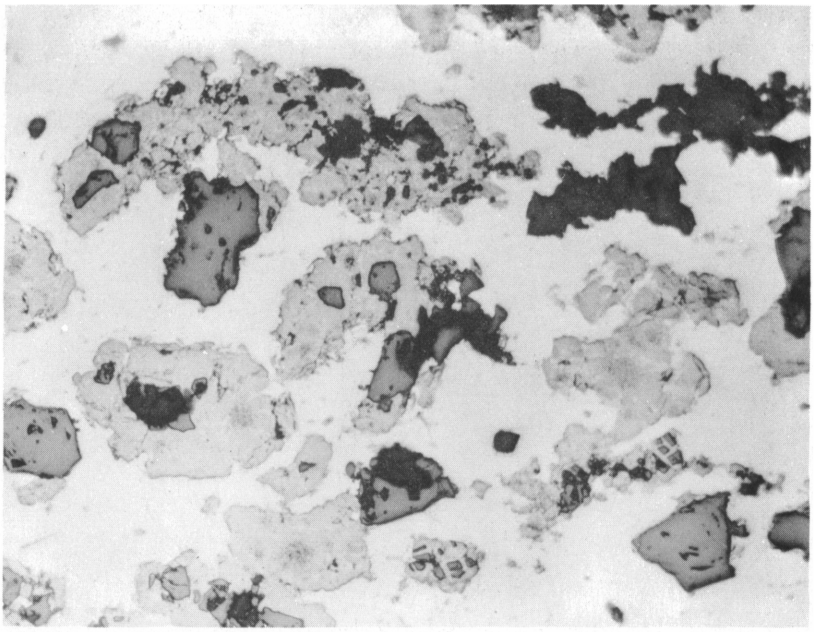

AS POLISHED 500X

Fig. 18 Microstructure of 42 weight percent UO_2 dispersed in aluminum heat treated at 590°C.

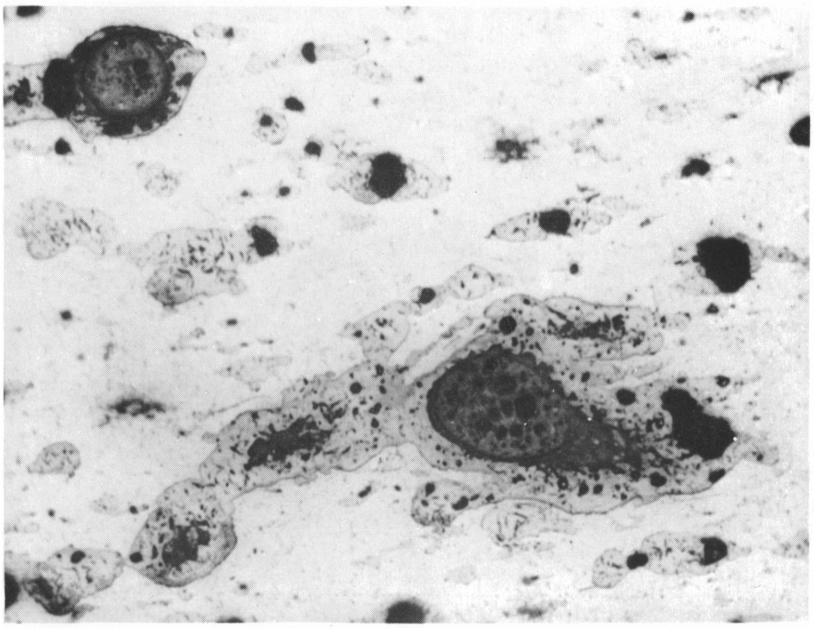

AS POLISHED 500X

Fig. 19 Microstructure of 24 weight percent UO_2 dispersed in aluminum irradiated to 45 weight percent burnup at ≈93°C.

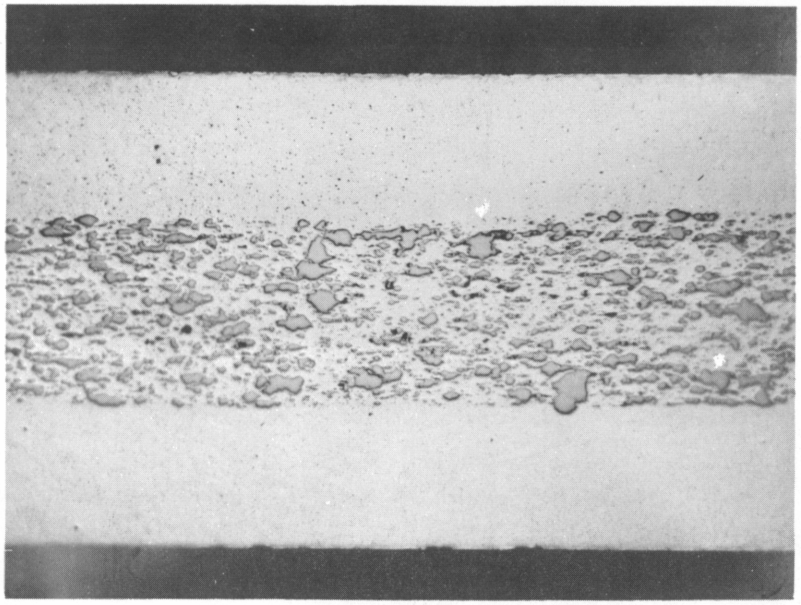

AS POLISHED 50X

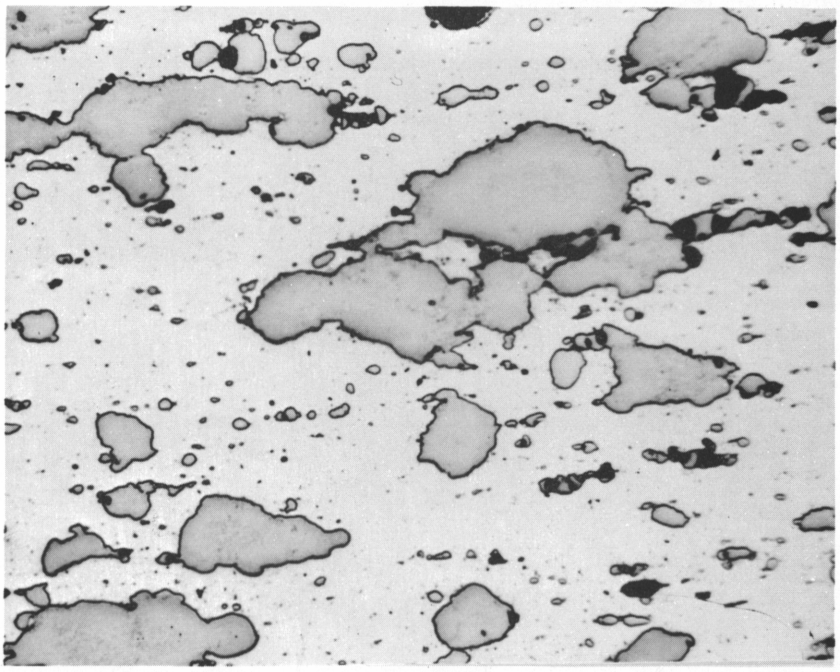

AS POLISHED 500X

Fig. 20 Microstructures of 24 weight percent UO_2 dispersed in aluminum irradiated to 18 percent burnup at 204°C.

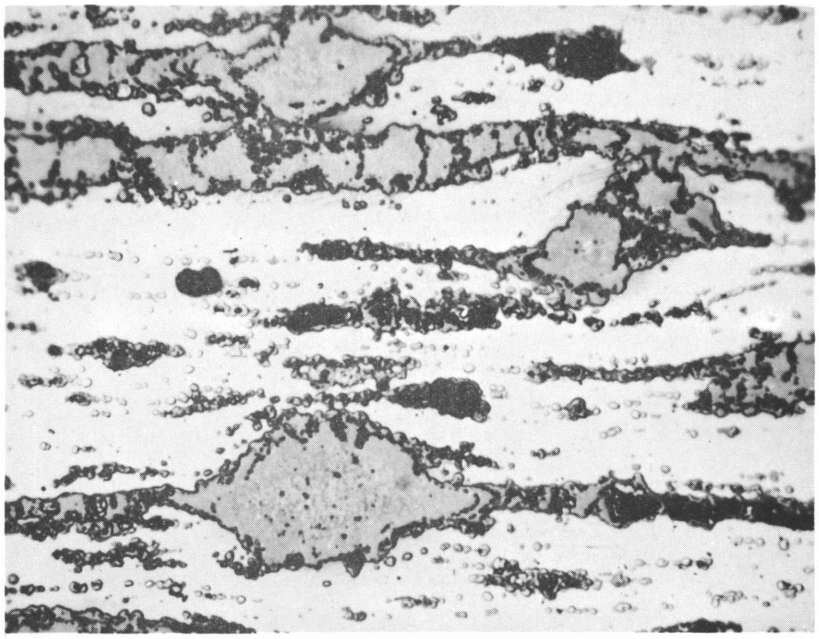

AS POLISHED 500X

Fig. 21 Microstructure of 22 weight percent U_3O_8 dispersed in aluminum irradiated between 175 and 204°C.

test plates (Figure 22) it is seen that the fuel particles are greatly increased in size during irradiation and are very similar in appearance to those seen previously in Figure 20. The particles which originally occupied 11 percent of the core volume grew until they comprized 45 to 50 percent of the core volume. This change in particle size is not reflected by corresponding changes in plate dimensions or density. In fact, the density changes on the ATR plates, with the exception of the blistered plates, were very little (this is contrary to lower temperature plate irradiations which show density decrease [7]). The matrix material is being consumed as the particles grow. In many instances the particles have grown across the core-clad interface giving the false appearance of core swelling.

The 35 weight percent U_3O_8 plates (having a U-235 content equivalent to the 32 weight percent UO_2 plates) show a similar increase in particle volume percent (15 percent before and 45 percent after irradiation) even though the reaction has not gone to completion (Figure 23). The U_3O_8 having greater quantities of oxygen present apparently requires more time and more aluminum to complete the reaction. Voids formed in the core are contained in the unreacted portions of the fuel particles and are still too small to cause core failure. None of the uranium oxide plates with the lower level fuel loadings developed blisters.

At the higher fuel loadings, 41 weight percent UO_2 and 44 weight percent U_3O_8, the core volume percent of the fully reacted particles reached 60 to 65 percent and 65 to 70 percent, respectively, from pre-irradiation volume percents of 16 and 21. With such a high ratio, core properties and stability obviously depend on these reacted particles.

The metallography of two of the blistered plates (one UO_2 and one U_3O_8) show that the particles became incompatible with the remaining matrix, and

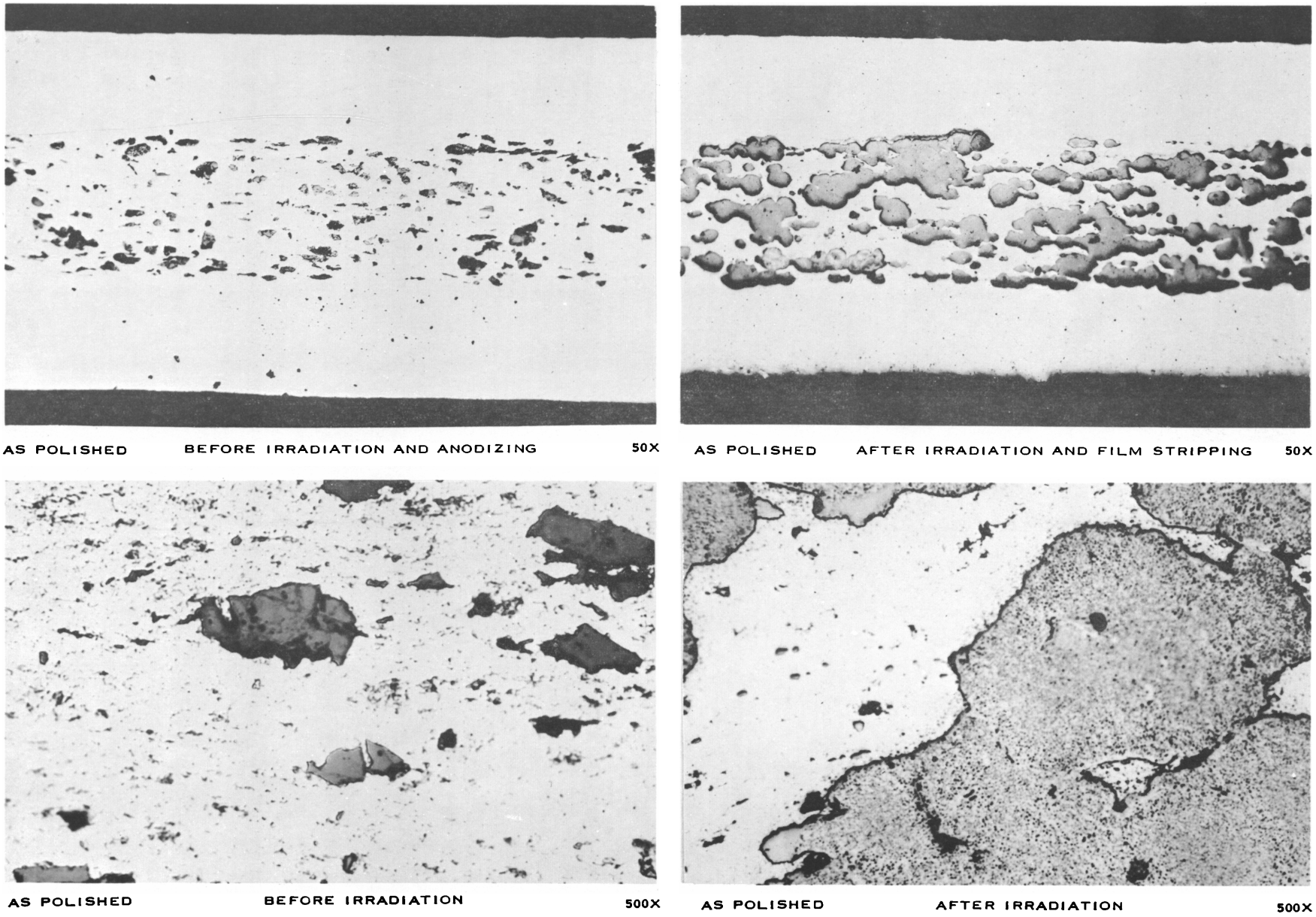

Fig. 22 Microstructures of 32 weight percent of UO_2 (ATR composition 8) before and after irradiation.

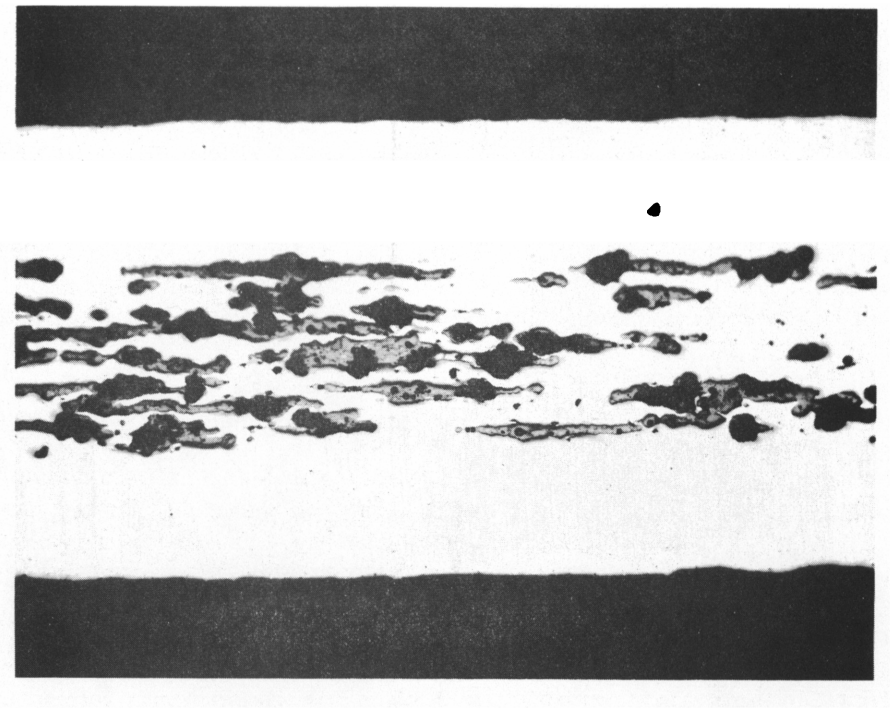

AS POLISHED 50X

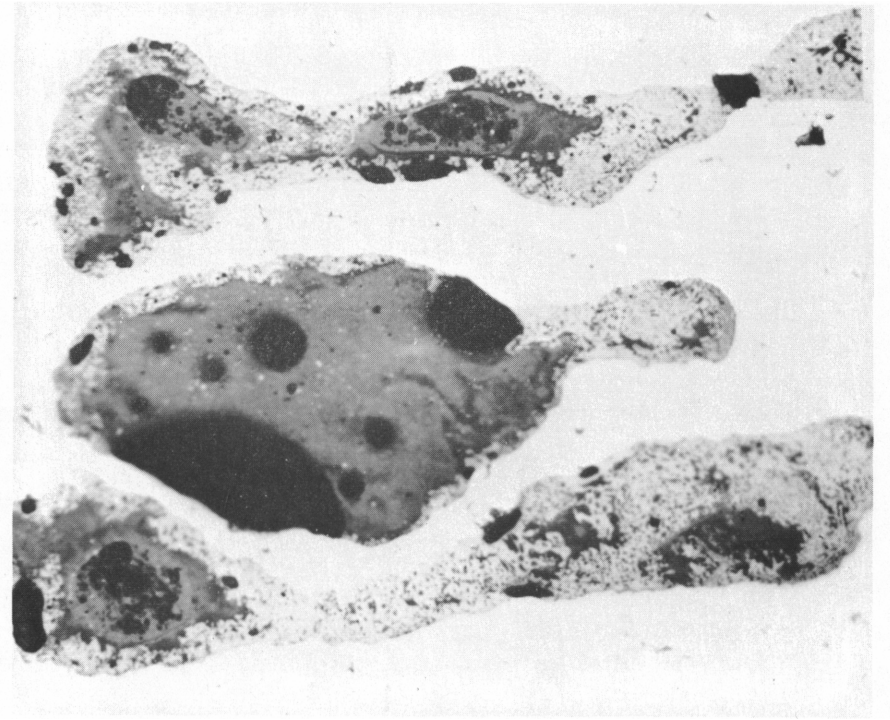

AS POLISHED 500X

Fig. 23 Microstructures of 35 weight percent U_3O_8 (ATR composition 7) after irradiation.

initiated cracks or voids large enough to be interconnected and cause blistering when diffusing fission gas entered. Figures 24 and 25 show at low magnification that separation took place in the cores of the plates and that large interconnecting voids had formed (in the cores) adjacent to the blisters. Details of the UO_2 blister (Figure 26-A) show a crack initiating at the edge of a fully reacted particle that had developed excessive porosity -- "swiss cheese effect". The matrix material (being only 35 volume percent of the core) was not strong enough to resist the swelling of this particle. Figure 26-B shows, in a crack that has widened considerably, particles are still touching both sides of the gap, indicating continued particle swelling. This mechanism of crack initiation and widening was typical of the 41 weight percent UO_2 plates. Figure 27 shows the similar effect in an area completely removed from the blister.

The mechanism of large void formation was different for the U_3O_8 plate. Detail metallography shows that separation occurred at the particle-matrix interface (Figure 28) forming a small pressure vessel which in some instances nearly surrounded the particle. When fission gases entered these relatively large area voids, the resulting force caused interconnecting and blistering. Again, this mechanism was typical throughout the 44 weight percent U_3O_8 plates (Figure 29).

The plane of weakness at the interface between the reacted U_3O_8 particle and the matrix can be explained if it is assumed that U_3O_8 reacts totally with Al to form UAl_4 and Al_2O_3 (attempts to analyze these constituents by X-ray diffraction found no crystallinity). If this reaction takes place there is a total volume decrease, ie, the volume of the products will only occupy 93 percent of the volume of the reactants. In other words, during reaction the matrix would be consumed faster than the particles grow. As the reaction progresses a particle may lose its share of matrix to an adjacent particle and cause separation at the over-stressed interface.

If a similar chemical reaction is assumed for UO_2, the volume of the products produced is still less than the volume of reactants (the volume of products are 98 percent of the reactants). But, the retention of fission gases within the reacted UO_2 particles is apparently sufficient to overcome this effect (as evidenced by the swiss cheese effect and indicated by fission gas diffusion coefficients: 10^{-18} through UO_2 and 10^{-15} through U_3O_8) so that particles swell.

One of the 44 weight percent U_3O_8 plates was removed at midcycle. The particle-matrix reaction was not complete at that time and there were no blisters. A three-point plot using starting, midcycyle, and final volume percents (Figure 30) indicates the rate of reaction at these particular conditions of time, temperature, fuel loading, and flux.

The failure mechanism of these high weight percent uranium oxide fuel plates can be summed up in the following steps.

(1) The uranium oxide particles reacted with the aluminum matrix material, consuming the matrix as the particles grew. The amount of matrix was reduced to as low as 30 volume percent of the core.

(2) Large voids formed in the core. In the case of the UO_2, these were caused by particles swelling to such an extent that cracks initiated and propagated in adjacent matrix. In the U_3O_8, separation occurred at a path of weakness (the particle-matrix interface)

AS POLISHED

≈ 20X

Fig. 24 Microstructure of 41 weight percent UO_2 (ATR composition 6) after irradiation, showing a blister cross section.

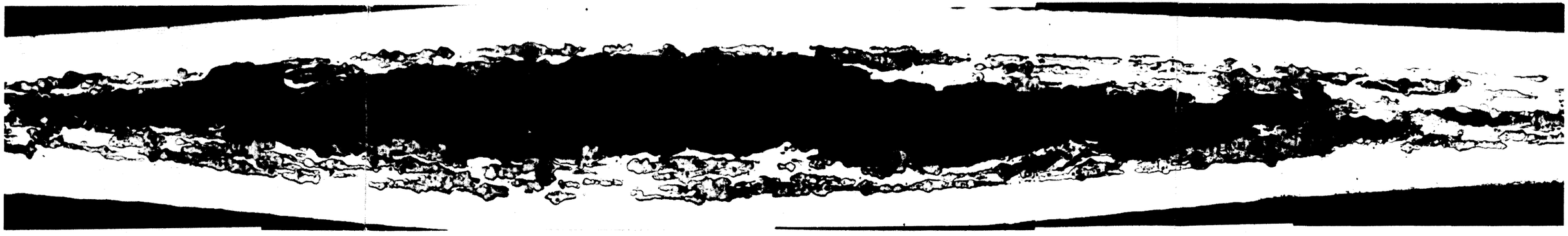

AS POLISHED

≈ 30X

Fig. 25 Microstructure of 44 weight percent U_3O_8 (ATR composition 5) after irradiation, showing a blister cross section.

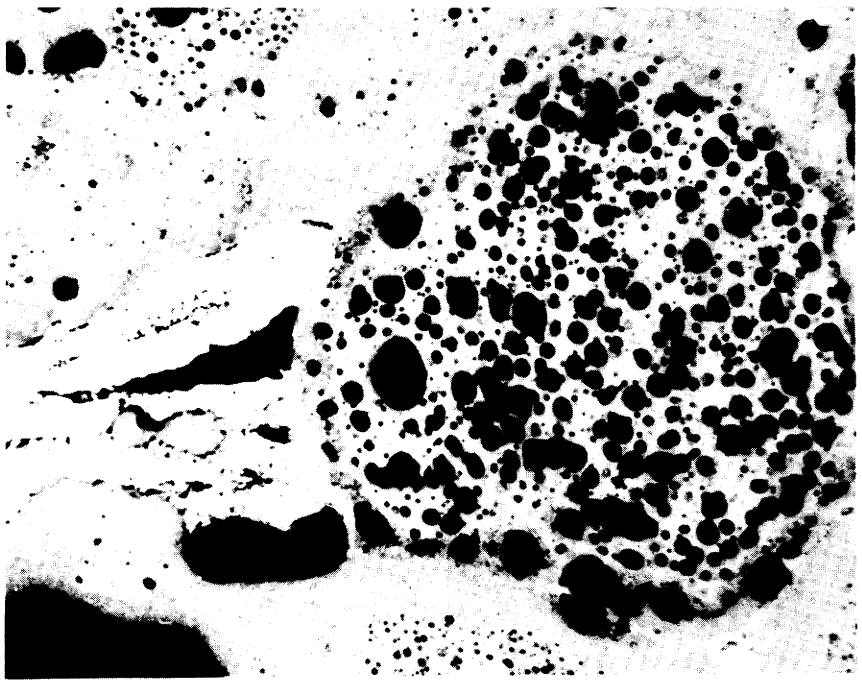

AS POLISHED 500X

A – CRACK INITIATED AT THE EDGE OF A SWELLING PARTICLE

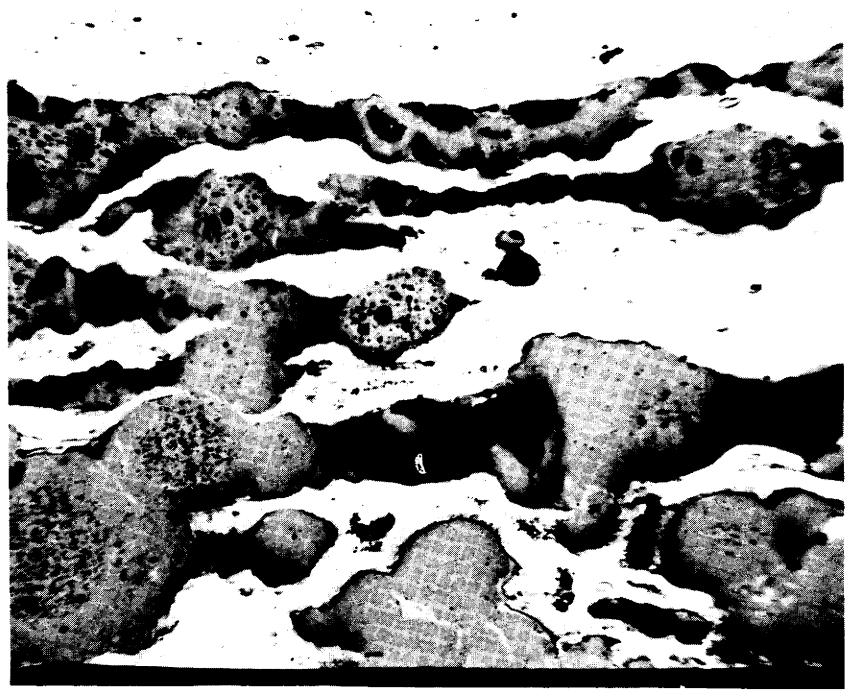

AS POLISHED 200X

B – CRACK WIDENING AIDED BY PARTICLE SWELLING

Fig. 26 Detail metallography in blister area of 41 weight percent UO_2 after irradiation.

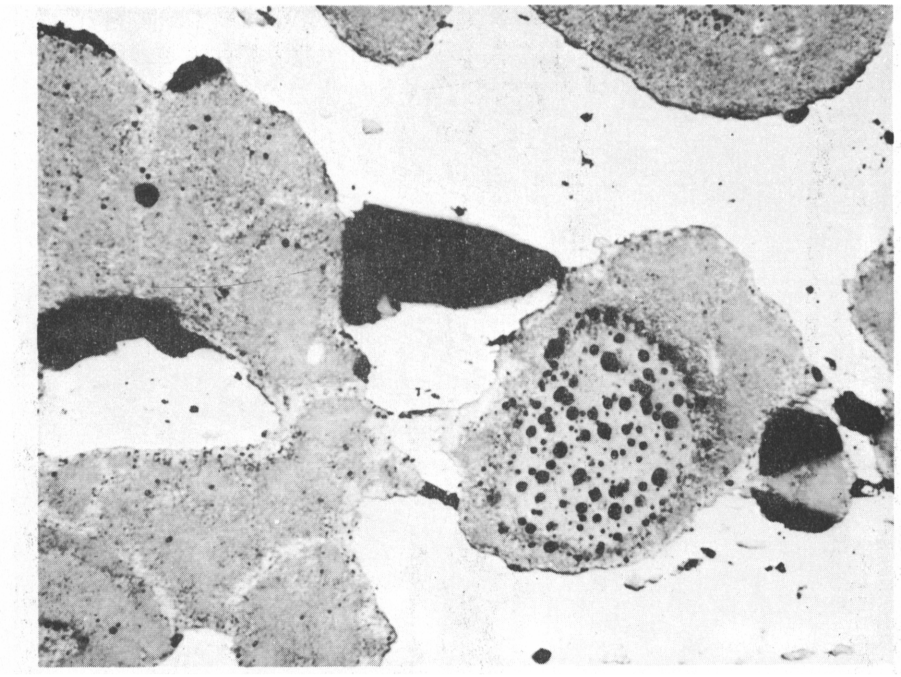

AS POLISHED 500X

Fig. 27 Microstructure of 41 weight percent UO_2 in an area removed from the blister.

which probably developed as a result of a total volume decrease in components during reaction.

(3) Fission gases collected in these large voids, to satisfy the relation between pressure and concentration [9], and exerted sufficient force to cause void interconnecting and blistering.

3. SUPERIOR PERFORMANCE OF UAl_3 PLATES

The 54 weight percent UAl_3 plates, having the same U-235 content and the same B_4C content as the 44 weight percent U_3O_8 plates (blistered plates) were placed in the same core position (same flux) with the same initial thermal barrier coating thickness. None of the irradiated UAl_3 plates blistered.

Metallography showed that voids formed in the UAl_3 plates remained small, spherical, and well dispersed. There was no mechanism of large void formation or interconnection (Figure 31), such as that in the UO_2 due to particle swelling, or in the U_3O_8 due to a probable total volume decrease during particle-matrix reaction.

The greater compatibility between the uranium-aluminum intermetallics and the aluminum matrix is understandable because the intermetallics are a product of reaction when uranium oxide in aluminum is thermally treated.

The compatibility of the intermetallics, as well as their better thermal conductivity, are the two principle reasons for the superior performance of these sample fuel plates. It should be noted, however, that UAl_3 does partially react during fabrication to form UAl_4. This can be seen in Figure 32. The dark

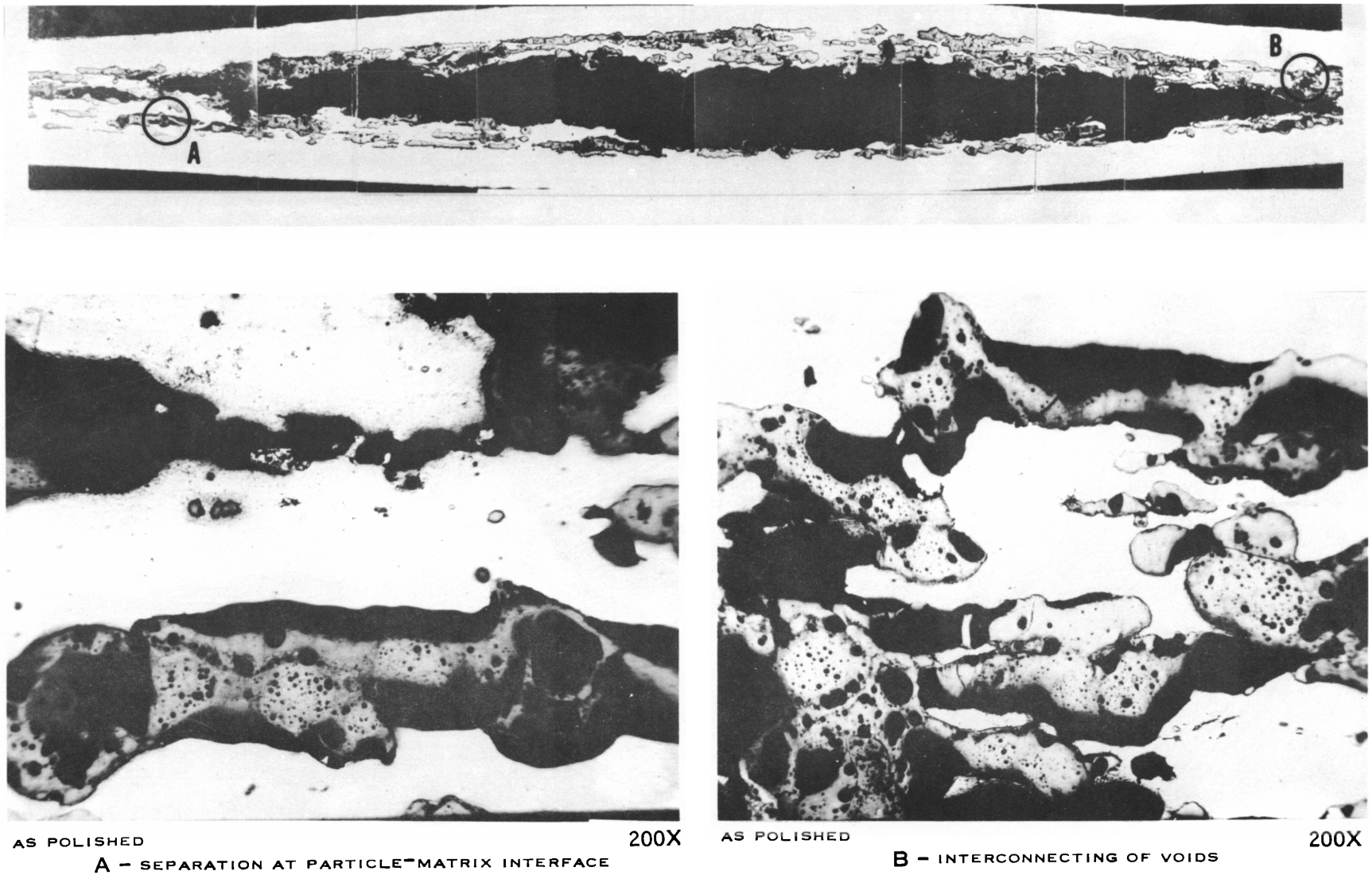

Fig. 28 Detail metallography in blister area of 44 weight percent U_3O_8 after irradiation

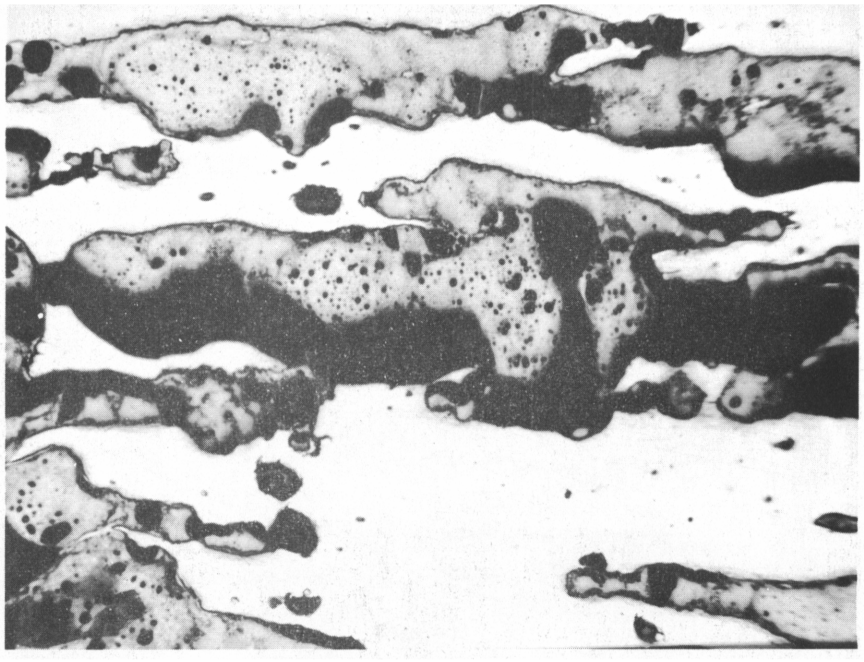

Fig. 29 Microstructure of 44 weight percent U_3O_8 in an area removed from the blister.

grey UAl_3 particles used as the fuel in this plate have reacted with the aluminum matrix material so that the particles are now surrounded with a light grey zone of UAl_4.

The thermal conductivities of UAl_3 and UAl_4 were estimated to be 0.63 and 0.72 watt/cm-°C. These estimates were made by extrapolation of the data for uranium--aluminum alloys and pure uranium metal. The thermal conductivity of unirradiated UO_2 is reported to be 0.08 watt/cm-°C while that of U_3O_8 is only 25 percent of this [10].

The higher thermal conductivity of the fuel plates containing UAl_3 allowed these plates to run cooler as evidenced by the hardness data (see Section V, 4.1, Hardness Tests). Thus the gas pressure in these plates was lower than in the plates containing uranium oxide fuels.

The sample fuel plates of compositions ETR 10 and 11, which were irradiated under ambient ETR condition, performed satisfactorily. This was to be expected.

Composition 10 had as core material a 22 weight percent uranium-aluminum alloy. Except for being without boron this is the normal ETR fuel plate core

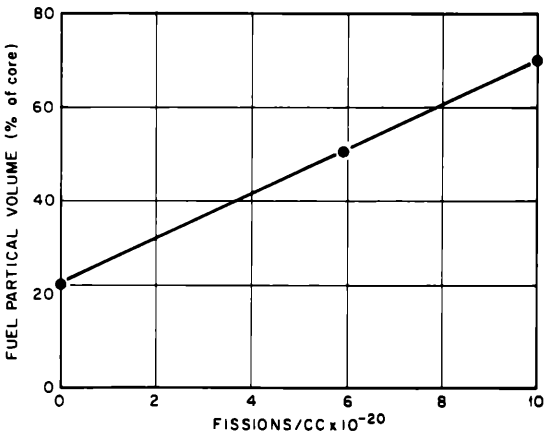

Fig. 30 Rate of reaction between U_3O_8 and aluminum in a 44 weight percent core.

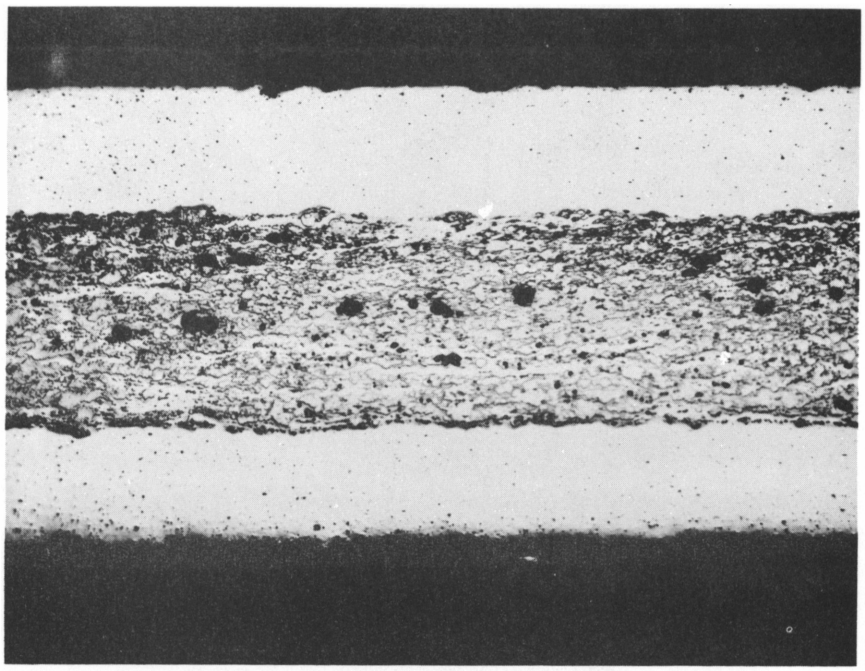

AS POLISHED 50X

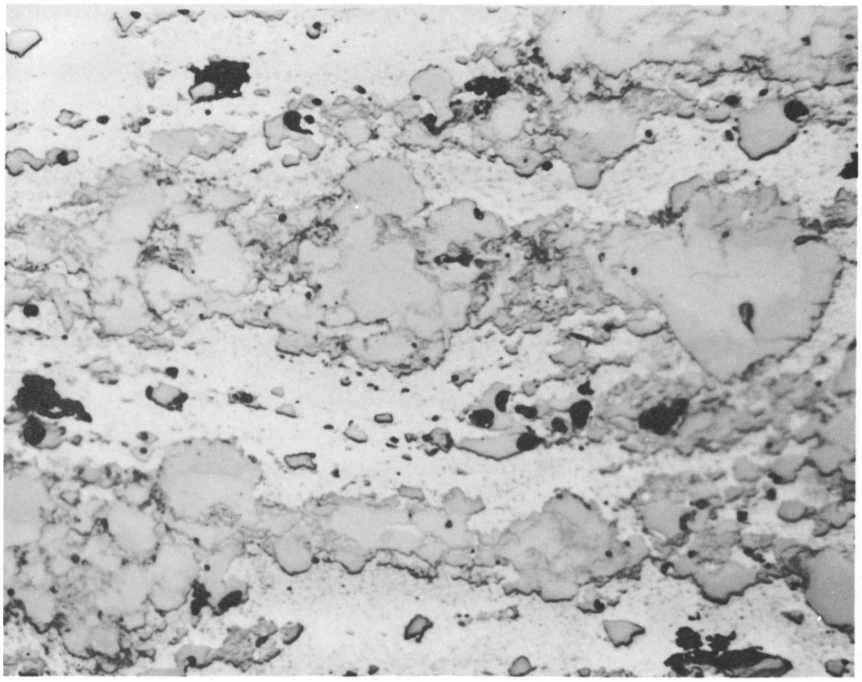

AS POLISHED 500X

Fig. 31 Microstructures of 54 weight percent of UAl_3 (ATR composition 4) after irradiation.

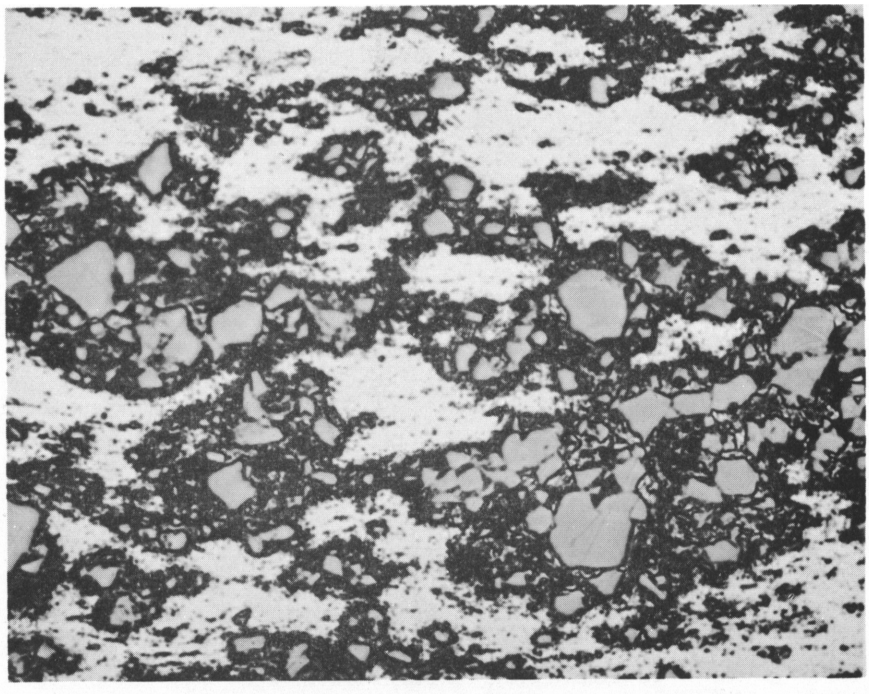

CHROMIC ETCH 500 X

Fig. 32 Microstructure of core of ATR sample fuel plate containing UAl_3.

material. ETR composition 11 fuel plates were made with 32 weight percent UAl_3 powder blended with aluminum powder core material and had the same U-235 content as the composition 10 plates. Plates of this type have been irradiated satisfactorily in the MTR.

A comparison of pre- and post-irradiation density and thickness measurements indicates that the irradiation stability of the two types of materials was nearly equal.

4. PHYSICAL AND MECHANICAL PROPERTIES

4.1 Hardness Tests

Hardness tests indicate that UAl_3 plate core ran cooler. Figure 33, a plot of matrix hardness vs fissions/cc (accomplished by variations in fuel loading), shows that irradiation hardening is taking place in the matrix of the UAl_3 cores while annealing of this effect (indicating higher temperatures) is taking place in the uranium oxide cores. Previous work, at MTR [6] conditions (lower temperatures), has shown that the amount of irradiation hardening in the matrix of the oxide plates is nearly equal to the hardening in plates with intermetallic dispersions.

Another interesting observation is the change in the 6061 cladding hardness with fissions/cc. The cladding hardness of both plate types (the oxide and intermetallic) fall within the same range and rate of decrease indicating that both plate types were at overaging conditions. The original DPN hardness of 51 was reduced to 30 during overaging (Figure 34).

Since the claddings of both plate types were at the same hardness condition (hence, the same strength) the fact that one type failed and the other did not, points again to a difference in core properties rather than cladding properties.

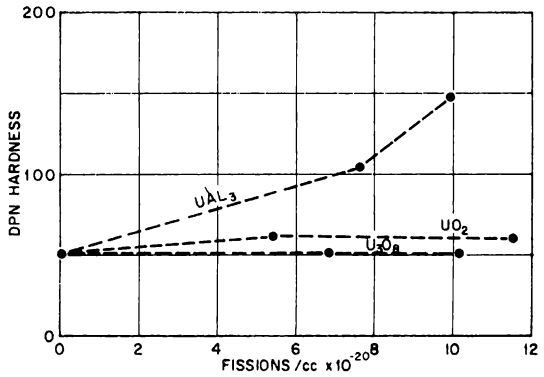

Fig. 33 Hardness changes in the X-8001 matrix material for the three core types.

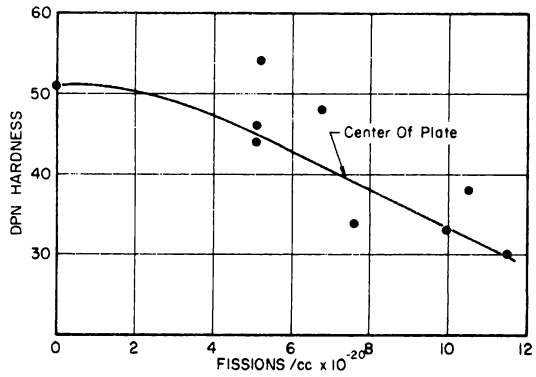

Fig. 34 Hardness changes in the 6061 cladding.

4.2 Densities

The plate densities were taken as fabricated, as anodized, after irradiation, ie, before and after film stripping (blistered plates were not stripped). With the exception of the blistered plates, the as-fabricated, as-anodized, and post-irradiation (after stripping) densities were all within one percent for any one plate. This is contrary to lower temperature plate irradiation experiments which show density decreases as a function of radiation.

The blistered plates, containing large voids throughout the core, exhibited density decreases of about three percent. The average densities of the various compositions (with coatings) before and after irradiation are listed for comparison with blistered plates, in Table XVI.

The reason for the low density changes in these elevated temperature irradiation plates is not fully understood; but it is likely a balance between void formation, particle-matrix reactions, greater mobility of voids (at elevated temperature) and the fact that the cores, being a product of powder metallurgy, are not 100 percent of theoretical density.

The results of the density measurements, plus the fact that particles grow across the core-clad interface consuming the cladding material and giving the false impression of core swelling, suggest that these measurements (density change and core thickening) are not effective means of evaluating radiation damage for these test conditions.

4.3 Bend Tests

A few post-irradiation bend test specimens were cut from a 40 weight percent UAl_3 plate and a 35 weight percent U_3O_8 plate. The specimens were bent to various angle increments over a 1.0 inch (diameter) mandrel to check core ductility. Both core types developed cracks between 5 and 15 degrees. Metallography of the two cores (Figure 35) shows that cracking in the uranium oxide core is associated with the fuel particles indicating a preferential path of weakness while the UAl_3 core cracks cross the matrix and particle with less selectivity. A five degree bend in one of these sample fuel plates would cause a deflection of 0.025 inch. Two plates bending toward each other by this amount would reduce the coolant channel considerably before core cracking would occur.

Although core ductility of irradiated plates with this fuel loading appears adequate (especially since the bend radius in service would be less severe) it should be determined for plates of higher loading in future evaluations.

TABLE XVI

DENSITIES OF ANODIZED FUEL PLATES BEFORE AND AFTER IRRADIATION

	Before Irradiation	After Irradiation
Composition 1 35 wt% U_3O_8	2.91	2.88
Composition 2 32 wt% UO_2	2.95	2.91
Composition 3 40 wt% UAl_3	2.91	2.87
Composition 4 54 wt% UAl_3	2.94	2.93
Composition 5 44 wt% U_3O_8	2.98	2.89 Blistered Plates
Composition 6 41 wt% UO_2	3.00	2.90 Blistered Plates
Composition 7 35 wt% U_3O_8	2.91	2.89
Composition 8 37 wt% UO_2	2.92	2.88
Composition 9 40 wt% UAl_3	2.91	2.88

4.4 Tensile Tests

The change in fuel plate strength during irradiation was determined for all but the failed compositions. Although the plates exhibited a decrease in hardness due to overaging in the 6061 and stress relieving of the cold worked X-8001 there was radiation strengthening of the lower weight percent plates (Table XVII). Even after elevating the temperature of the post-irradiation test samples to 204°C, the strengths were still equal to the pre-irradiation room temperature strengths.

The higher weight percent composition (the only composition post-irradiation tested was 54 weight percent UAl_3), having a post-irradiation cladding hardness as low as annealed 6061, showed a 15 percent decrease in room temperature strength.

These tests indicate that deterioration had not occurred in any of the lower weight percent fuel plate compositions. The decrease in strength of the higher weight percent UAl_3 plate, the only fuel type of high loading that did not fail, re-emphasizes the need for fuel-matrix compatibility.

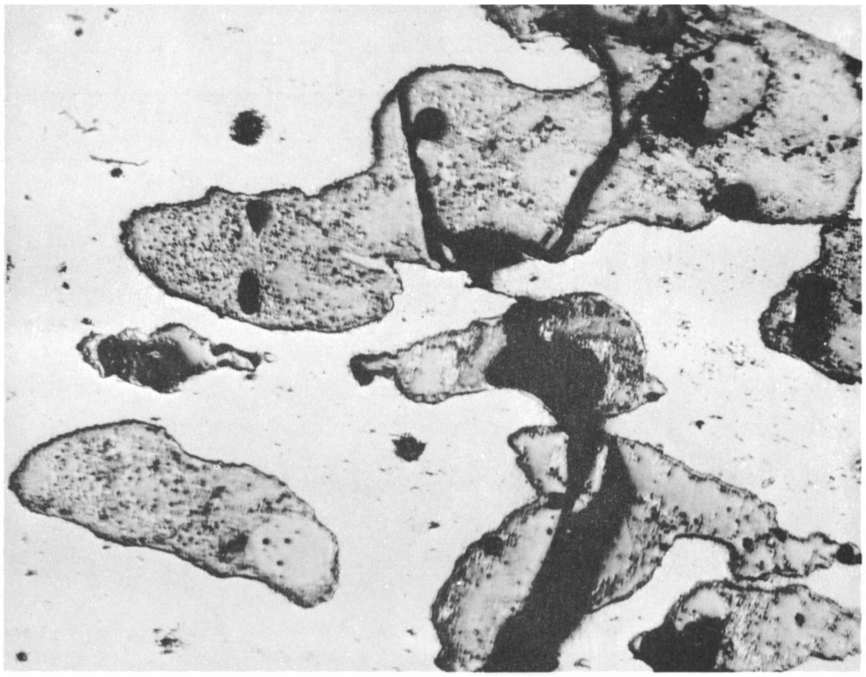

AS POLISHED 350X

35 WT U_3O_8

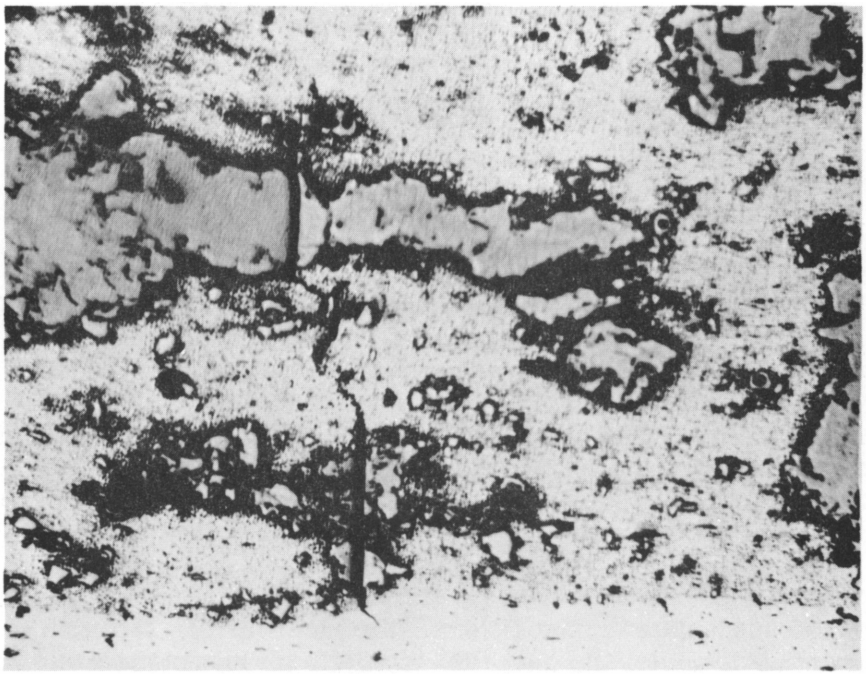

AS POLISHED 350X

40 WT UAL_3

Fig. 35 Metallography of bend test specimens.

TABLE XVII

THE CHANGE IN ROOM TEMPERATURE TENSILE STRENGTH OF THE VARIOUS FUEL PLATES DURING IRRADIATION

Composition	Change in Strength (%)
35 wt% U_3O_8 clad with X-8001	+16
32 wt% UO_2 clad with X-8001	+14
40 wt% UAl_3 clad with X-8001	+50
35 wt% U_3O_8 clad with 6061	+58
32 wt% UO_2 clad with 6061	+23
40 wt% UAl_3 clad with 6061	+45

5. ELECTROLYZED COATINGS

Six nonfueled test platelets of stainless steel and six of 6061 aluminum alloy were chrome plated by a process called "Electrolyzing". It was hoped that the anti-gall properties and the anti-corrosion properties would be enhanced.

The plates were exposed to reactor conditions similar to the fuel test plates. As might be expected, the stainless plates did not deteriorate (Figure 36), but a dissimilar metal corrosion cell was established between the aluminum and its chrome plating (Figure 37). The aluminum acts as a sacrificial anode to protect the chromium, and corrodes much faster than uncoated aluminum.

An additional set of cylindrical electrolyzed samples was exposed to the reactor environment in another ETR position (I-13 NE) during cycle 57. The results were similar to the plates--the stainless samples did not pit but the aluminum samples did. Some of the aluminum cylindrical samples electrolyzed by a modified process (eliminating the need for an organic bath) showed a more localized attack. The two aluminum cylindrical types are shown in Figure 38 after irradiation.

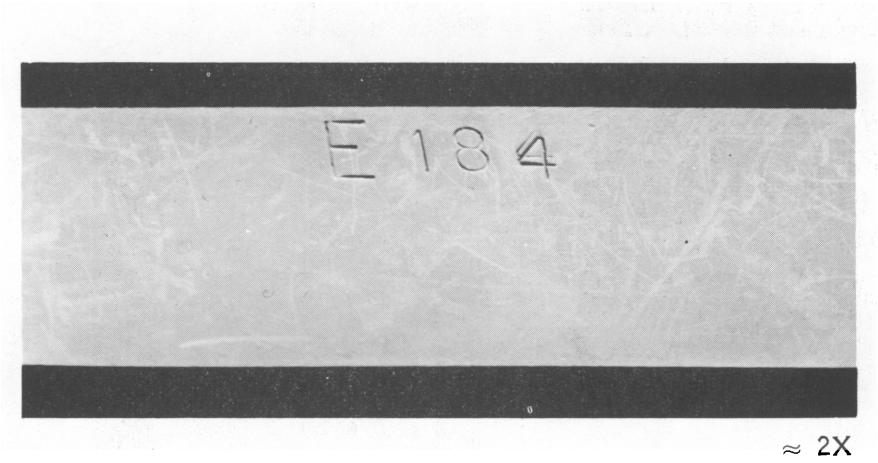

Fig. 36 Photograph of electrolyzed stainless steel plate.

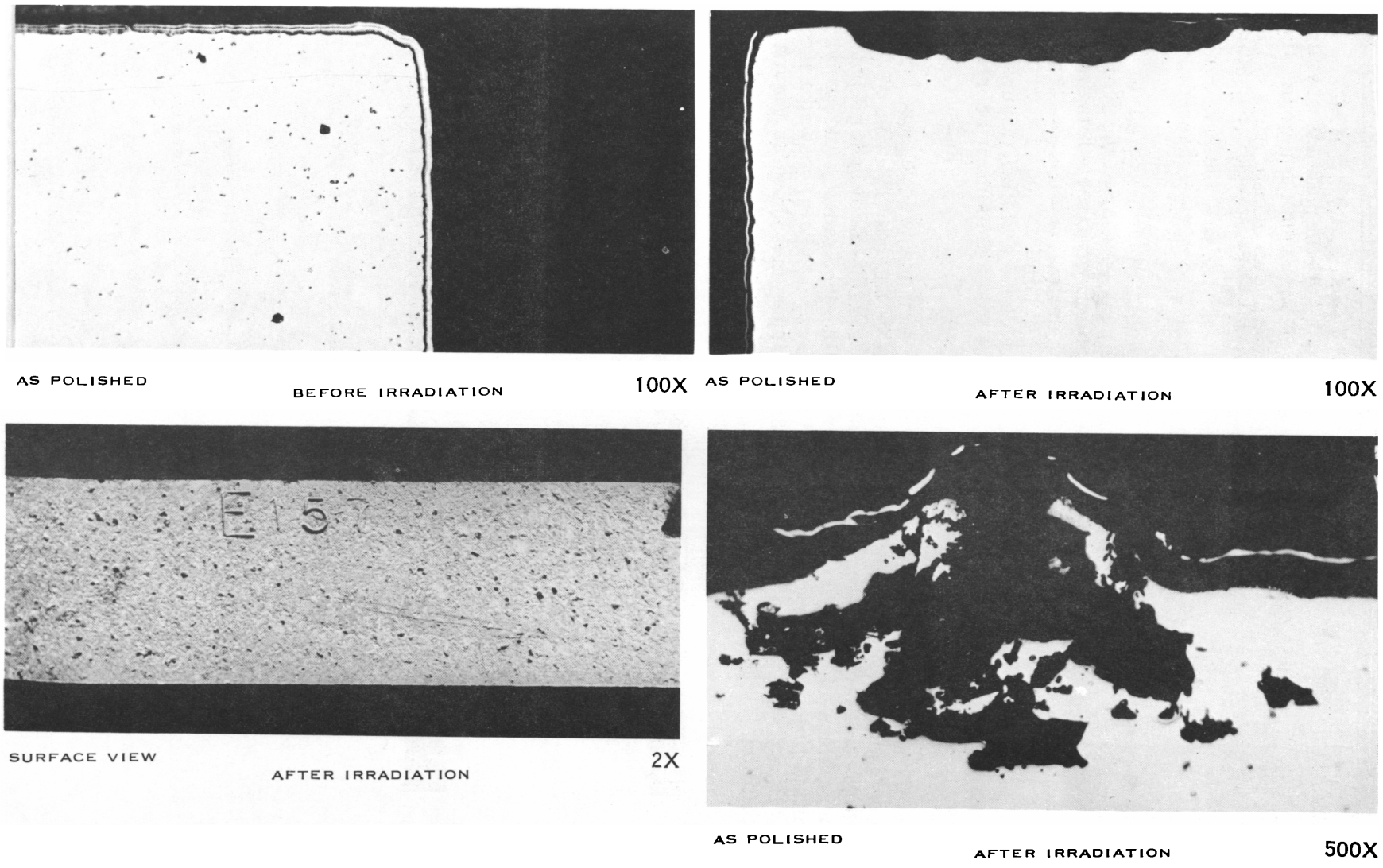

Fig. 37 Electrolyzed aluminum plates before and after irradiation.

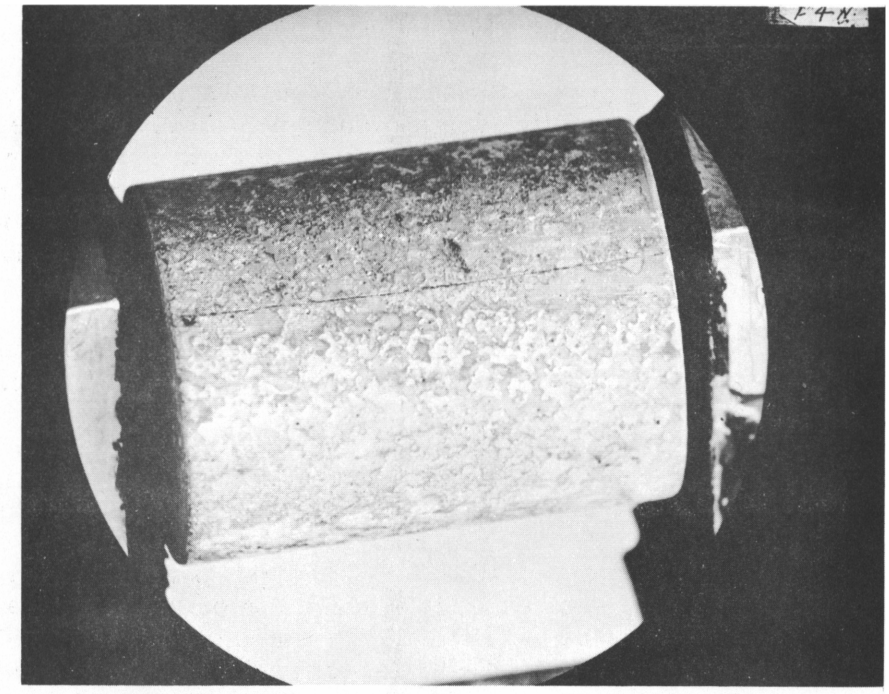

MODIFIED PROCESS ≈ 1X

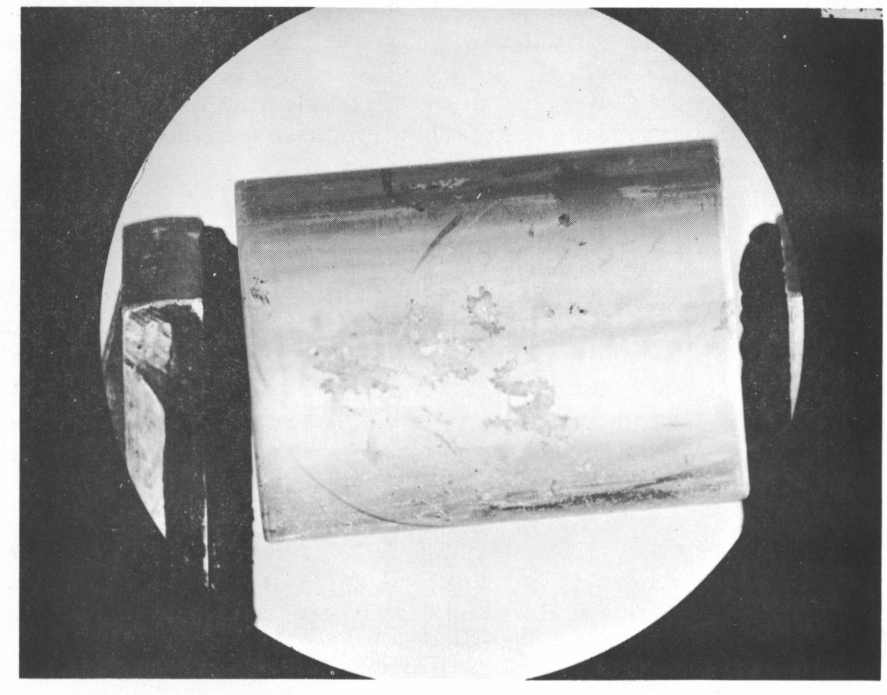

STANDARD PROCESS ≈ 1X

Fig. 38 Two types of electrolyzed aluminum cylinders after irradiation.

VI. CONCLUSIONS

Because of the many areas of uncertainty always present in irradiation programs, even the most carefully designed and scientifically analyzed experiments frequently result in enigmas. How much more so this is true in surveillance and proof-testing. There remains unsolved in the ATR irradiation experiment a good estimate of the temperature attained by the coated specimens. Uncertainties in coating thickness, composition, and thermal conductivity make the assignment of a realistic temperature most difficult.

There are several areas, however, which do appear quite conclusive as a result of the test evaluation. There is substantial evidence in support of the following statements:

(1) A reference U_3O_8-Al fuel is satisfactorily stable under radiation at temperatures up to about 204°C to a burnup of 6×10^{20} fiss/cc.

(2) High weight percent U_3O_8 (>40 weight percent U_3O_8) in aluminum fuel plates, when exposed to a high fission rate at surface temperatures in the order of 230 to 290°C is subject to failure in the range of burnup of $> 10 \times 10^{20}$ fiss/cc. It is interesting to note (although extrapolations may be dangerous) that this material sustained gross damage without catastrophic failure.

(3) The failure mechanism appears to be the buildup of fission product gas in the voids around particles with the resulting internal pressure fracturing the matrix to form a blister and ultimately (it may be assumed) rupturing.

(4) UAl_3 fuel irradiated under the same conditions to the same level of burnup did not fail and did not even appear excessively damaged.

(5) Because of its better thermal conductivity the UAl_3 fuel cores did not reach as high temperatures as the oxide fuels.

(6) Anodized coatings on aluminum for protection or thermal barrier present some unresolved problems under irradiation. It is obvious that some coating remained after irradiation but the degree of film stripping appears to vary with thickness, temperature, and type of aluminum. The irradiated coating varied in appearance from smooth to pitted, in composition from amorphous to boehmite, and generally showed some increase in thickness over the initial value.

(7) The effect of irradiation on the thermal conductivity of anodized coatings is not known. Very limited work indicates the thermal conductivity of anodized aluminum coatings may be decreased by irradiation.

(8) Aluminum, electrolyzed by the Rochelle salt-zinc prefilming process, has little corrosion resistance during irradiation in a water environment. All samples were badly spalled after exposures of 4×10^{20} n/cm^2 (>1 MeV).

(9) Aluminum electrolyzed by zinc prefilming in an inorganic bath offers some improvement over the original process but shows some localized corrosion at 4 x 10^{20} n/cm^2 (>1 MeV).

(10) Electrolyzed stainless steel appears to be stable under the same conditions. Coupons exposed to 8 - 9 x 10^{20} n/cm^2 (> 1 MeV) were still satisfactory.

On the basis of these tests uranium oxide dispersed in aluminum appears satisfactory for some reactor use but it is necessary to recognize that this material combination has a definite upper limit of performance and that this limit is in the vicinity of ATR design conditions.

VII. FUTURE WORK

If all of the sample fuel compositions had successfully survived this irradiation, it is likely that U_3O_8 would have been accepted as the fuel for the ATR regardless of the uncertainty in the test temperature.

Since failures occurred in both U_3O_8 and UO_2 compositions, oxide fuel for ATR must either be completely rejected for UAl_3 or tests must be repeated under more closely controlled conditions. With the large investment in U_3O_8 on the part of both ATR and HFIR and the present unknown engineering feasibility of the UAl_3 fuel, the logical approach seems to be an additional test. As was pointed out in the early meetings on the subject there is only one way of establishing the ATR test parameters with some certainty and that is by means of a loop test. The design of such a loop is currently in progress with the following objectives:

Maximum Heat Flux	2.25×10^6 Btu/hr-ft^2
Coolant Velocity	35 - 45 ft/sec
Maximum Thermal Flux	3.8×10^{14} μ/cm2-sec
Initial Specimen Surface Temperature	170°C
Pressure at Maximum Heat Flux	400 psia
pH	5.0

Details of the sample program are not yet firm but most likely will include the following materials:

Core Materials	U_3O_8, UAl_3, UO_2 (with B_4C)
Fuel Loading	31 - 55 weight percent U_3O_8 equivalent (X-8001 matrix)
Cladding	6061 - 0
Final Specimen Temperature	$\approx$ 220°C
Roll Reduction	vary 8:1 to 18:1
Burnup	$\approx 7 \times 10^{20}$ fiss/cc 1 cycle
Maximum	$\approx 12 \times 10^{20}$ fiss/cc 2 cycle

The current schedule for this work calls for completion of construction of the loop during the last quarter of FY 1964 and completion of irradiation early in FY 1965.

VIII. REFERENCES

1. D.R. deBoisblanc et al, The Advanced Test Reactor - ATR Final Conceptual Design, IDO-16667 (November 1960).

2. W.C. Francis and S.E. Craig, Progress Report on Fuel Element Development and Associated Projects, IDO-16574 (August 16, 1960).

3. L. Young, Anodic Oxide Films, New York: Academic Press, 1961.

4. J.C. Griess et al, Test Relative to the Advanced Test Reactor and Correlation with Previous Results, Part IV, ORNL (to be published).

5. D.L. Keller, "Predicting Burnup of Stainless-UO_2 Cermet Fuels", NUCLEONICS 19, No. 6 (June 1961) pp 45-48.

6. G.W. Gibson and W.C. Francis, Annual Progress Report on Fuel Element Development for FY 1962, IDO-16799 (August 15, 1962).

7. G.W. Gibson, M.J. Graber, and W.C. Francis, Annual Progress Report on Fuel Elements Development for FY 1963, IDO-16934 (November 25, 1963).

8. S. Timoshenko, Theory of Plates and Shells, First Edition, New York: McGraw-Hill Book Company, Inc., 1940.

9. A.R. Kaufmann, Nuclear Reactor Fuel Elements; Metallurgy and Fabrication, New York: Interscience Publishers, 1962.

10. J. Belle (ed.), Uranium Dioxide: Properties and Nuclear Applications, (Division of Reactor Development, AEC) 1961, p 739.

11. J.E. Cunningham et al, Fuel Dispersion in Aluminum-Base Elements for Research Reactors, TID-7546 (November 1957) pp 269-297.

12. J. Williams, Dispersion-Type Fuel Elements Based on Fissile Ceramics, TID-7546 (November 1957) pp 554-562.

PHILLIPS
PETROLEUM
COMPANY

ATOMIC ENERGY DIVISION